RAYLEIGH WAVE TOMOGRAPHY OF TEXAS

FROM AMBIENT SEISMIC NOISE

A Thesis Presented to

the Faculty of the Department of Earth and Atmospheric Sciences

University of Houston

In Partial Fulfillment

of the Requirements for the Degree

Master of Science

By

Yao Yao

May 2013

Rayleigh wave tomography of Texas from ambient seismic noise

Yao Yao

Approved

Dr. Aibing Li

Dr. Guoquan Wang

Dr. Dale Bird

Dean, College of Natural Sciences and Mathematics

Acknowledgements

First of all, I would like to extend my sincere gratitude to my supervisor, Dr. Aibing Li, for her instructive advice and patient guidance throughout my Master's degree. I am deeply grateful of her help in completion of this thesis.

Secondly, I would like to express my heartfelt gratitude to my thesis committee, Dr. Dale Bird and Dr. Guoquan Wang, for their encouragement and insightful suggestions.

Also, I owe my gratitude to my friends and my fellow classmates for enjoying these two years times of living abroad together. I owe special gratitude for Duo Yuan and Lun Li, who are always willing to help and discuss the tough questions I encounter.

Finally, I should give my most sincere gratitude to my beloved grandmother, my parents, and my whole family, who have always been helping me out of difficulties and understanding me without a word of complaint, for their assisting, supporting, and caring for me all of my life.

RAYLEIGH WAVE TOMOGRAPHY OF TEXAS

FROM AMBIENT SEISMIC NOISE

An Abstract of a Thesis Presented to

the Faculty of the Department of Earth and Atmospheric Sciences

University of Houston

In Partial Fulfillment

of the Requirements for the Degree

Master of Science

By

Yao Yao

May 2013

ABSTRACT

Texas has been one of the leading states in petroleum production since the discovery of the Spindletop oil field in 1901. Despite its huge economic value of petroleum and numerous geophysical explorations in several oil fields, the crustal structure of the Texas is not well studied. This thesis aims to investigate crustal structure in central and eastern Texas using seismic ambient noise data recorded at 87 broad-band stations from the Transportable Array of the USArray network between March 2010 and February 2011.

Seismic observations based on cross-correlations of long ambient noise sequences between pairs of stations are used to obtain phase velocities at periods from 6 s to 40 s. Phase velocity maps show that positive anomaly area coincides with Laurentia craton crust and the negative anomaly area coincides with continental margin crust. The boundary between positive and negative anomaly is perfectly consistent with the Ouachita belt.

From the inversion of phase velocity results, we construct 1-D and 3-D shear-wave model with four crust layers and one mantle layer. In the 3-D shear-wave velocity model, the high velocity province is imaged in central and northwestern Texas with the highest velocity beneath the Llano Uplift. This pattern extends across the whole crustal depth, reflecting cold cratonic crust in general and igneous influence at the Llano Uplift. The lowest velocity appears in northeastern and southeastern Texas at shallow crust, correlating with thick sediment layers. In deep crust and upper mantle, the lowest velocity is confined in southeastern Texas at the continental margin. Ouachita orogen could have brought old oceanic crust that contained large amount of water to the lower crust and upper mantle.

CONTENTS

List of Figures

1. INTRODUCTION

Texas has been one of the leading states in petroleum production since the discovery of the Spindletop oil field in 1901. Oil and natural gas are found in most parts of the Texas, which has produced more oil and natural gas than any other state. Texas has been explored or drilled more heavily than all states or any other region worldwide. In August 2003, 151,605 active oil wells and 66,951 active gas wells produce oil and natural gas in the state (Bureau of Economic Geology, 2005) (Figure 1). Despite its huge economic value of petroleum and numerous geophysical explorations in several oil fields, the crustal structure of the Texas is not well studied.

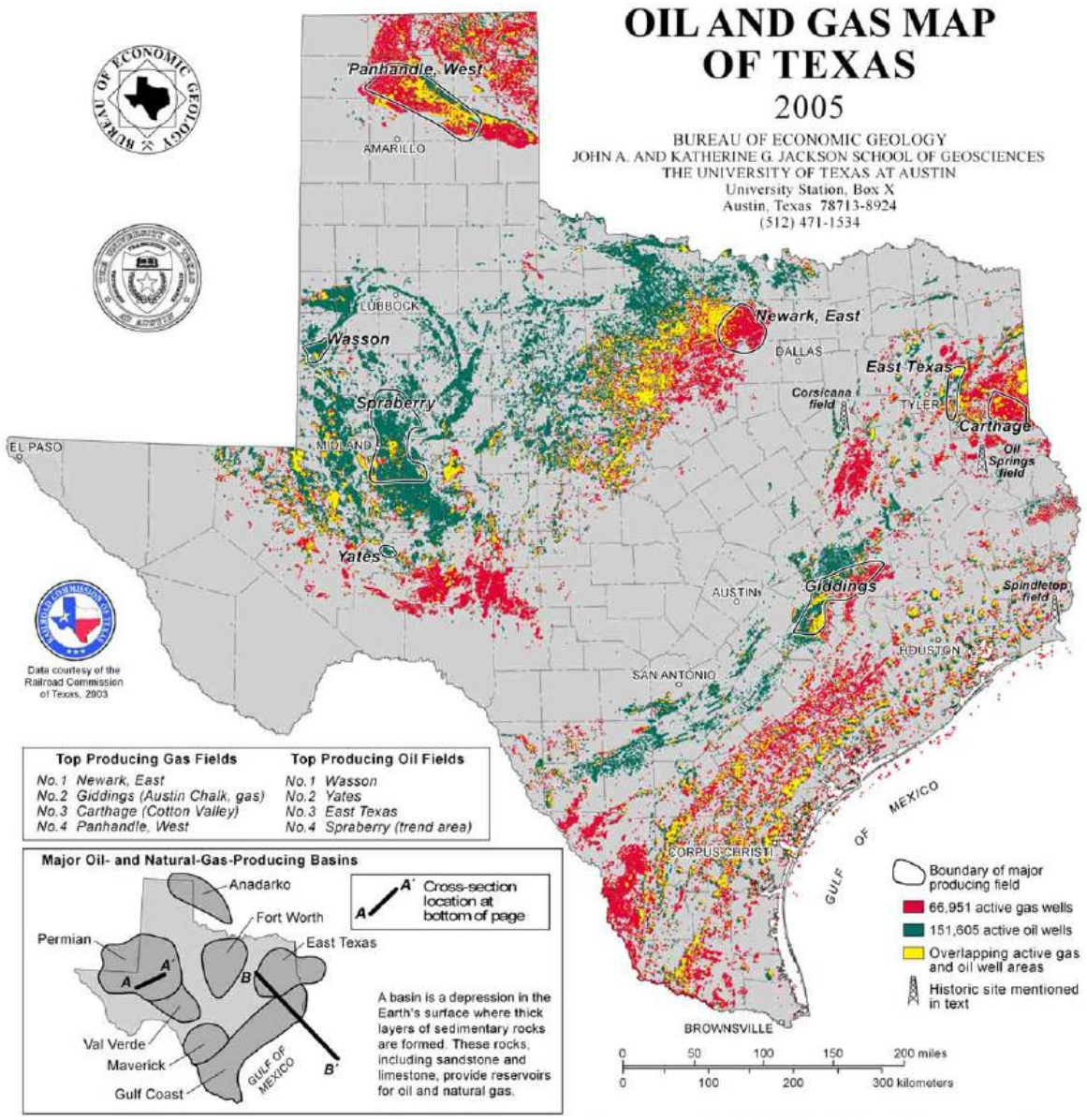

Figure 1- The Oil and Gas Map of Texas, 2005. (Bureau of Economic Geology, The University of Texas at Austin)

Texas has been affected by several tectonic cycles consisting of continental collision and rifting. Basically, according to the Tectonic Map of Texas (1997) (Figure 2), there are three principal tectonic cycles:

(1) Precambrian cycles are recorded in the ancient rocks of the Llano region and near Van Hom and El Paso. The famous one is the Llano cycle of Between 1,200 and 1,080 million years ago (mya).

(2) The Paleozoic Ouachitan cycles began with continental rifting about 550 mya and end about 245 mya. This cycle closed with the collision of south and North America, which caused the Ouachita orogeny. There are two major features recorded this Ouachitan history. The first one is the foreland area of West Texas. This signifies that the structure of this area is shaped by a nearby mountain belt. The other one is the ancient and almost entirely eroded mountain belt which lay south and east of the Ouachita tectonic front. It's mostly buried roots extend from the Marathon area of West Texas, where deeply eroded relics of the mountain belt are exposed, through a great northward-curving arc to near Dallas, thence into Oklahoma.

(3) The current tectonic cycle in Texas is the Gulf Coast. It began in Texas in the Late Triassic about 220 mya with continental rifting and led to creation of oceanic crust in the Gulf of Mexico. The tectonic evolution of the Gulf of Mexico continental margin is characterized by two Wilson cycles, i.e., repeated episodes of opening and closing of ocean basins along the same structural trend (Figure 3). This evolution includes (1) the Precambrian Grenville orogeny; (2) formation of a rift-transform margin during late Precambrian opening of the Iapetus Ocean; (3) the late Paleozoic Ouachita orogeny during assembly of Pangea; and (4) Mesozoic rifting during opening of the Gulf of Mexico (Huerta and Harry, 2012).

The area north and northwest of the Ouachita system has typical cratonic crust in terms of thickness and velocity (Mitchell and Landisman, 1970). And the crust of the Gulf Coast region is complex due to the interaction of Paleozoic plate convergence with Mesozoic rifting (Keller et al., 1989).

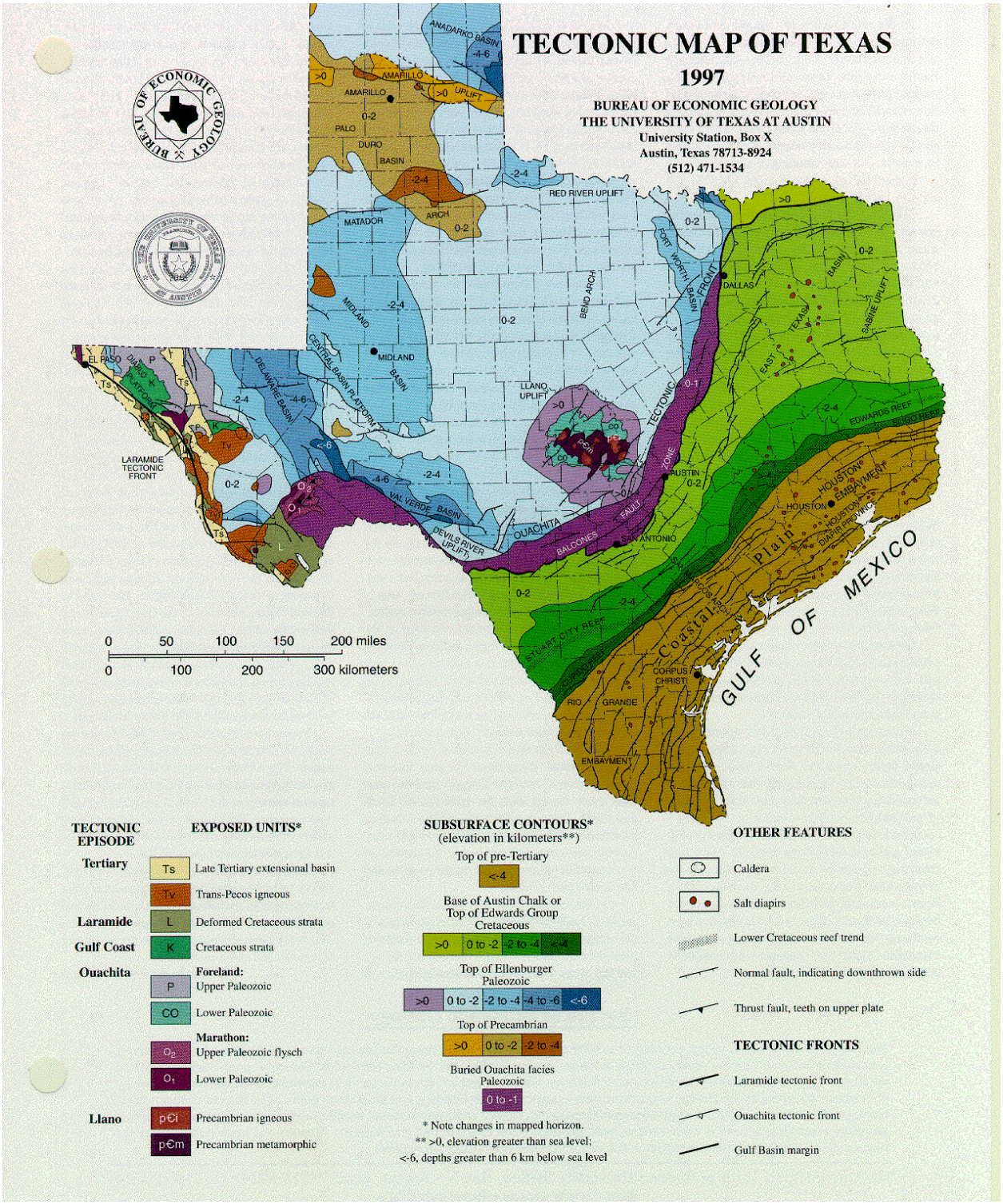

Figure 2- Tectonic Map of Texas, 1997. (Bureau of Economic Geology, The University of Texas at Austin)

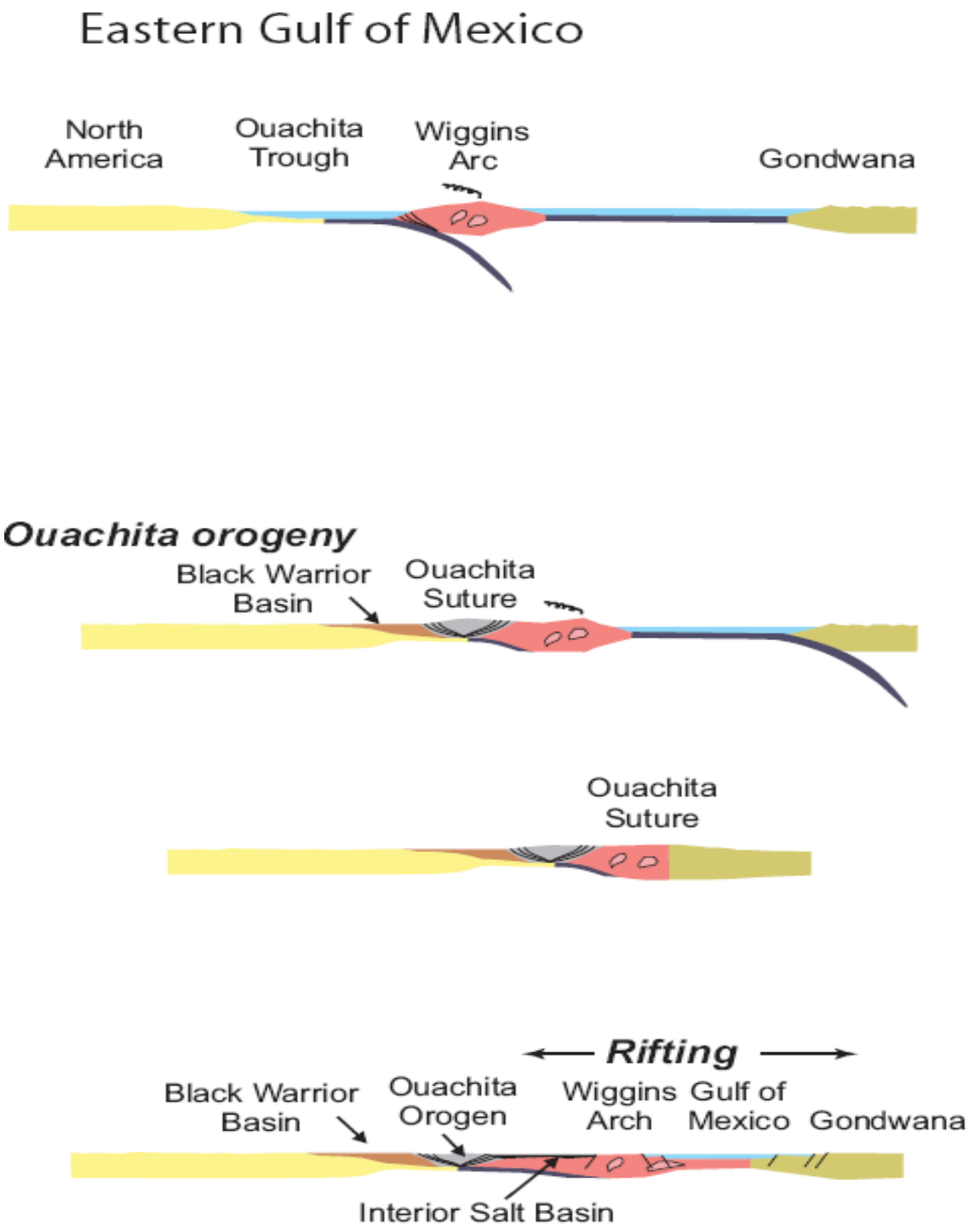

Figure 3- Tectonic evolution of the Mississippi Gulf of Mexico margin and Ouachita orogeny. (Huerta and Harry, 2012)

The Llano uplift of central Texas consists of multiply deformed, Mesoproterozoic metasedimentary, metavolcanic, and metaplutonic rocks intruded by late syntectonic to post-tectonic granites (Figure 4) (Mosher, 2008). The evolution of the Llano Uplift can be showed by tectonic model for Grenville orogeny along southern margin of Laurentia (Figure 5) (Mosher, 2008). In Figure 5, step A shows subduction with southward polarity was active before 1150 mya. Step B illustrates collision resulting in juxtaposition of lithotectonic domains including exotic arc and overriding of arc by southern continent, plus internal imbrication and interleaving of ophiolitic rocks. Subduction of Laurentian margin resulted in high-pressure metamorphism of continental crust at depth, buoyant rise of coherent fragments of subducted continental crust, and jamming of subduction zone. In step C, thermal structure re-equilibrated after being perturbed by overall orogenic thickening and increase in temperatures. Step D is exhumation accomplished by erosion and extension. It contained slab breakoff and its consequences like further uplift, upwelling of asthenosphere, and underplating of basaltic magmas, leading to intrusion of late syntectonic juvenile granites. In step E, continued compression along strike in west Texas causes further shortening, deforming oldest late granites (Mosher, 2008).

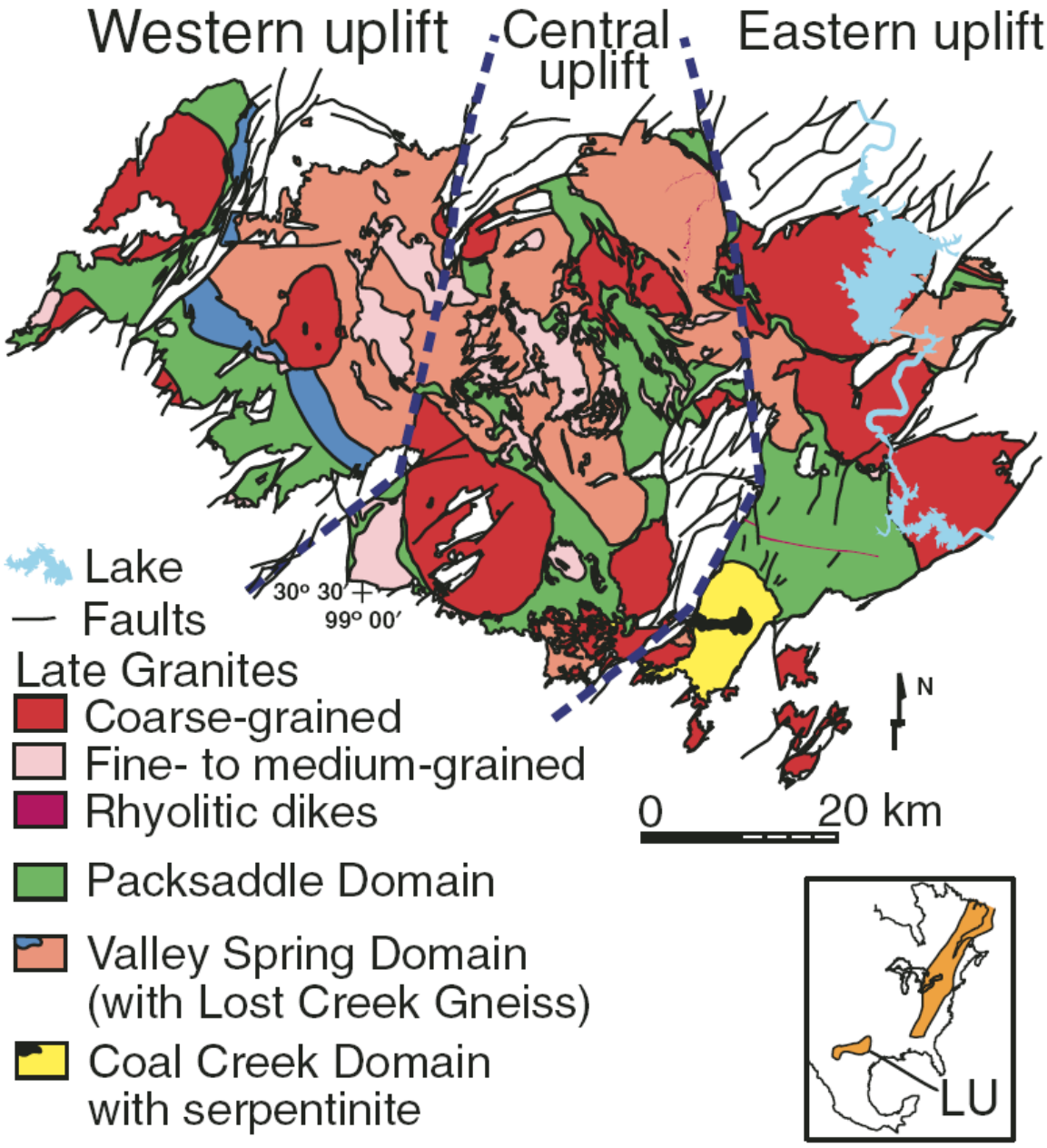

Figure 4- Geologic map of Llano Uplift (LU) of central Texas. Boundaries between western, central, and eastern portions of uplift are shown (dashed dark blue lines). Inset shows surface and subsurface location of Grenville orogenic belt in North America. (Mosher, 2008)

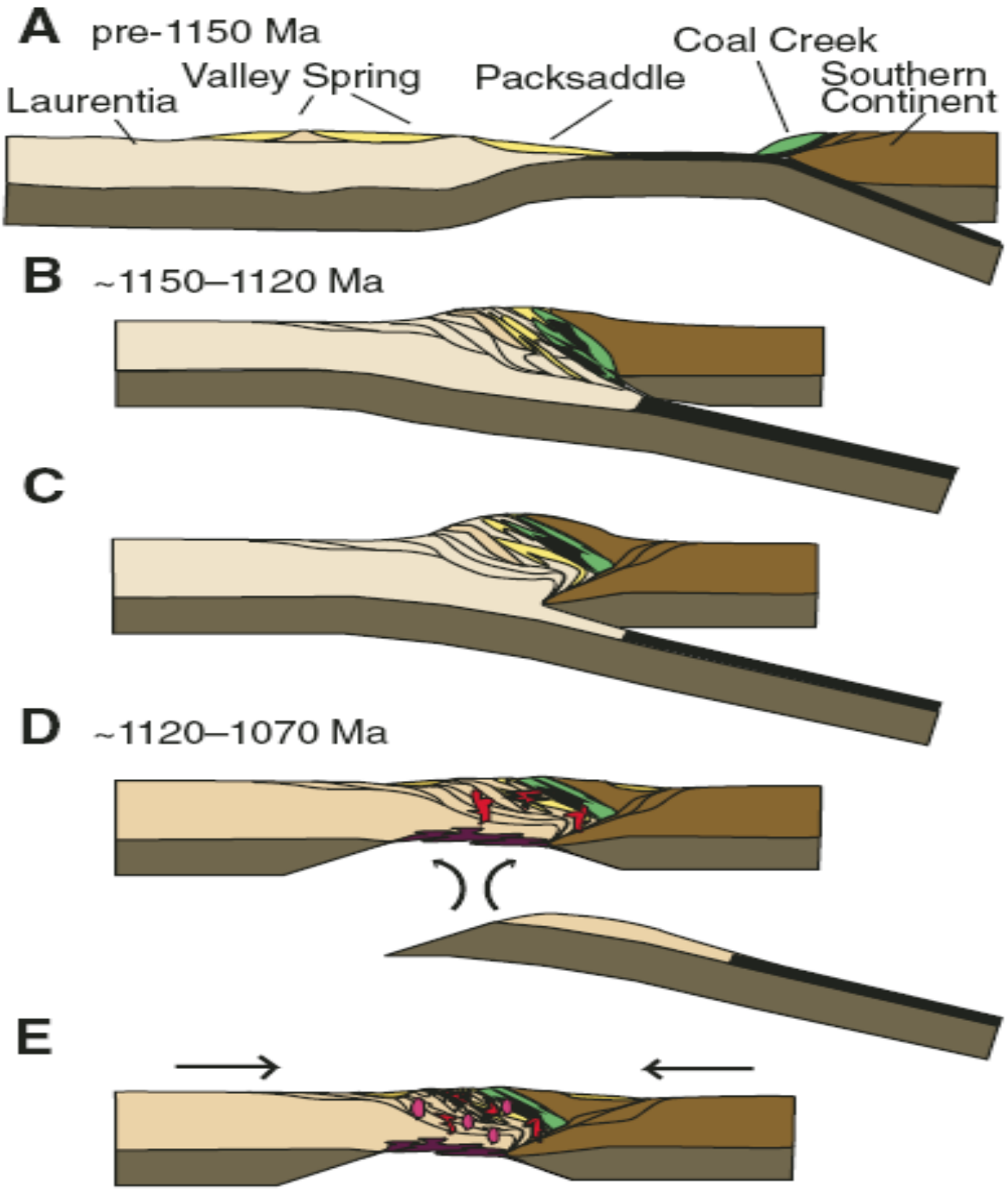

Figure 5- Tectonic model for Grenville orogeny along southern margin of Laurentia, showing evolution of Llano Uplift. (Mosher, 2008)

The Ouachita System is a Paleozoic geosyncline and orogenic belt which borders the southern edge of the central United States craton. The foldbelt extends more than 2,100 km from near the southern terminus of the Appalachians to western Texas, where it passes into Mexico (Figure 6) (Nicholas and Rozendal, 1975). The Ouachita Mountains were formed during a cycle of opening and closing of the Iapetus Sea (Figure 7) (Housknecht, 1986). The Ouachita System is characterized by large-scale, north-to-west-directed overthrusting (Evans and Zoerb, 1984) that caused considerable involvement of the basement in the uplifts (Benton, Broken Bow, Waco, and Devils River) that these uplifts have a different origin from the Llano Uplift. The Waco Uplift is in east-central Texas named by the nearby city. It is a 130-km-long and 16-km-wide northeast-trending, doubly plunging anticlinal complex cresting at a depth of about 7 km and has been defined by seismic mapping and confirmed by the drilling of the Shell 1 Barrett well in Hill County, Texas. This uplift is about 40 km behind the leading edge of the Ouachita facies rocks (Nicholas and Rozendal, 1975).

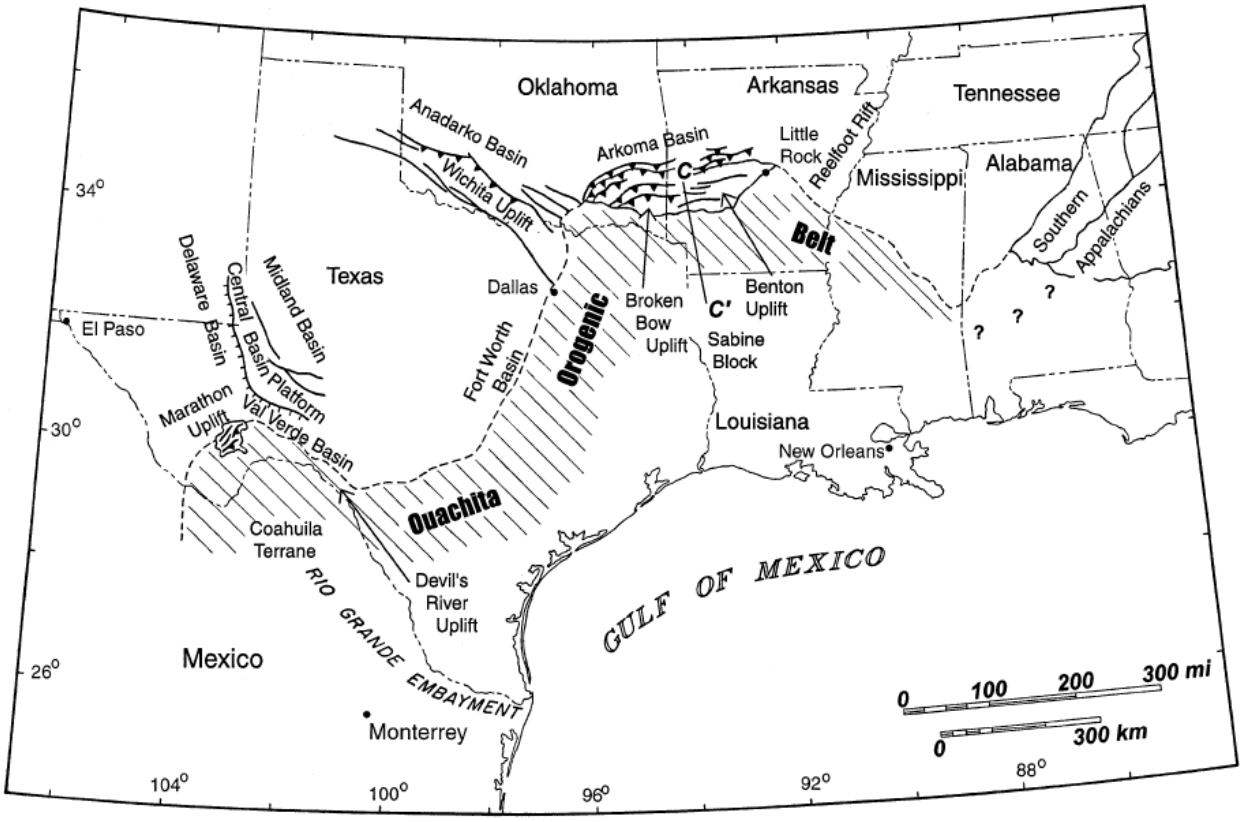

Figure 6- Tectonic map of the Ouachita Orogen. (Keller et al., 1989)

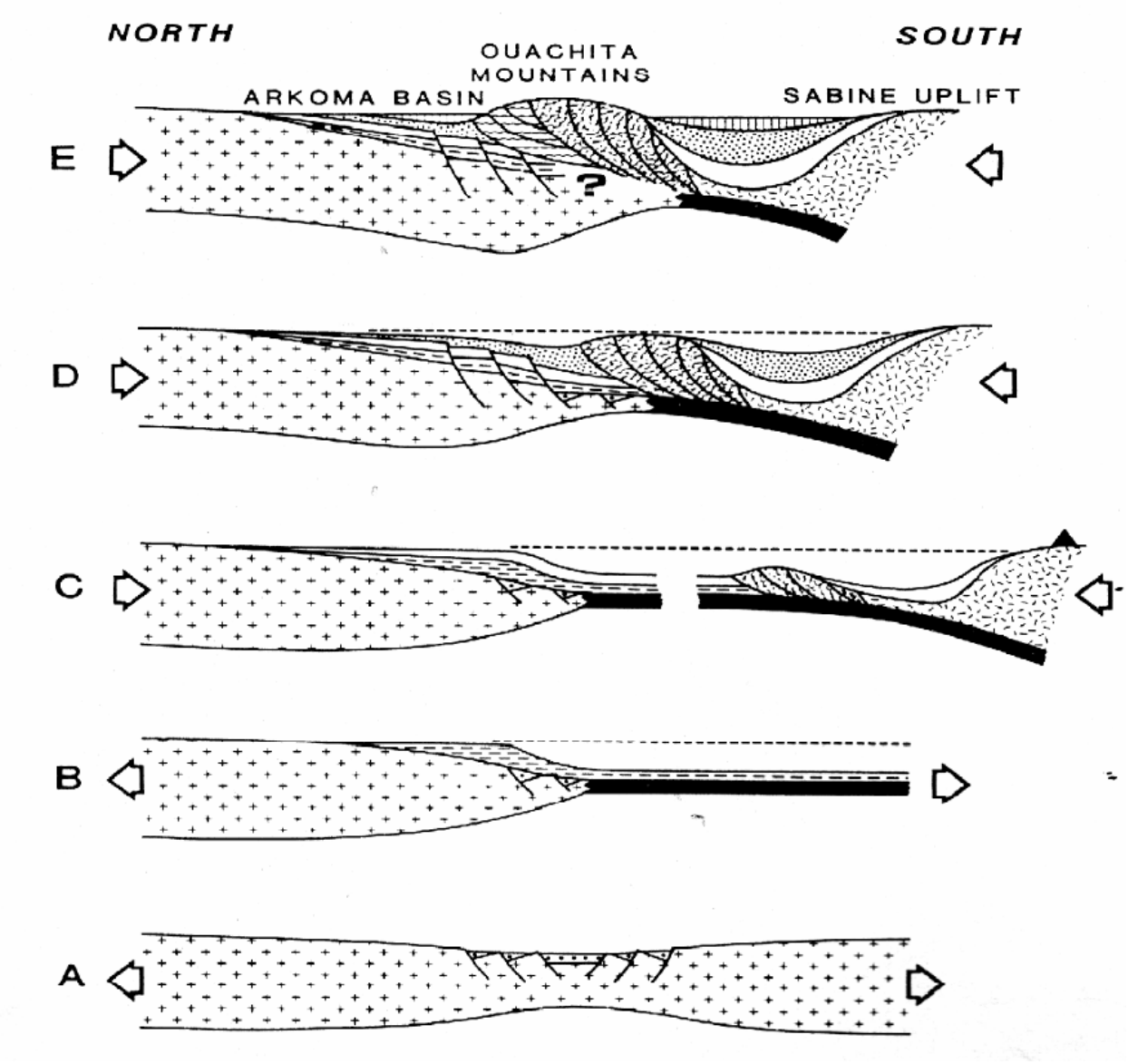

Figure 7- The progression of a complete Wilson Cycle beginning with Precambrian rifting of the North American continent. (A), followed by successive oceanic crust formation (B), convergent plate motion between North America and the colliding body forming a subduction zone (C), plate collision (D), and finally uplift of the Ouachita Mountains and formation of the Arkoma foreland basin (E). (Houseknecht, 1986)

The Gulf of Mexico continental margin is similar to the U.S. Atlantic margin in that the axis of Mesozoic continental breakup trended subparallel to the buried middle Paleozoic Ouachita fold-and-thrust belt (Pindell and Dewey, 1982; Salvador, 1991; Thomas, 1976, 1991). Since the main targets of geologic setting including the Llano Uplift, Ouachita Belt and the Coastal Margin of Gulf of Mexico locate in central and eastern Texas, the primary objective of this research is to construct a high-resolution crustal model of central and eastern Texas by utilizing ambient seismic noise tomography, which can constrain surface wave phase velocity maps at short periods (6-40 s) and provide more detailed and higher resolution on 3-D crustal structure. Seismic noise data are required from the IRIS data management center (www.iris.edu) utilizing Transportable Array Stations of the USArray.

Using ambient seismic noise has several advantages compared with traditional seismic methods. (1) Inversions used in traditional seismic methods require some a priori information about the source, which is not always known very accurately. For ambient noise, the source information is not of concern. (2) Earthquake surface wave data are from averages over extensive long distances or large areas thence they limit the resolution of resulting seismic images. In contrary, seismic noise data are determined by the distance between stations and can be improved with dense seismic network. (3) Traditional teleseismic methods are difficult to deal with short periods (below 40 s) of surface wave dispersion. With ambient seismic noise, short period waves can be robustly sampled from 6 s to 40 s. (4) Ambient seismic noise can provide higher vertical and horizontal resolution to map the crustal structure compared to traditional seismic tomographic methods.

Because Rayleigh waves are primarily sensitive to shear-wave velocity, the main objective is to build shear-wave velocity model for central and eastern Texas.

In order to achieve the objective, the research is carried out by following the sequence of steps:

1) Request the TA stations data for one entire year from IRIS since March 2010 to February 2011.

2) Process the Rayleigh wave from TA stations data using Ambient Seismic Noise Method.

3) Construct fundamental mode Rayleigh wave phase velocity maps at different period (6 s, 8 s, 10 s, 12 s, 14 s, 16 s, 18 s, 20 s, 25 s, 30 s, 35 s and 40 s).

4) Obtain 3-D shear-wave crust and upper mantle structure.

5) Discuss the results and their tectonic implications.

With the development of the new crust model of Texas, several questions show below will be addressed.

1) Is the crustal structure at depth correlate with surface geological features?

2) Is there an anomaly high shear-wave velocity associated with the Llano Uplift and how deep of the top and bottom of it?

3) Is there a crustal root beneath the eroded Ouachita orogeny?

4) Is the Mexico rifting margin a volcanically or non-volcanically margin?

2. Previous Studies

Since Texas has been one of the leading places in petroleum production over the world, it has been a long history for geologic and geophysical study in Texas and its vicinity area. Early crustal scale seismic studies in Texas was include seismic reflection, refraction, and surface wave researches in central Texas (Prewitt, 1969), the Gulf Coast region south of Ouachita system (Cram, 1962; Hales et al., 1970; Dorman et al., 1972; Keller and Shurbet, 1975).

Refraction and surface wave data (Mitchell and Landisman, 1970; Prewitt, 1969; Stewart, 1968) indicate that the cratonic areas north and northwest of the Ouachita system are typical of continental crust in terms of thickness and its velocity structure. Seismic reflection data (Nicholas and Rozendal, 1975; Nelson et al., 1982; Lillie et al., 1983; Evans and Zoerb, 1984) indicate that the Ouachita system is characterized by large-scale, north-to-west directed overthrusting. The Gulf Coast region south of the Ouachita system is a key area in attempts to decipher Paleozoic tectonic events (Kruger et al., 1989). The complex crustal structure indicated by refraction and surface wave data (Cram, 1962; Warren et al., 1966; Hales et al., 1970, Keller and Shurbet, 1975) reflects the complex tectonic history of this region. However, previous seismic studies in Texas are either small scale or low resolution due to the limit of the data sets. With the large amount of data from the Transportable Array of the USArray in Texas, high resolution, state-wide models can be developed.

This ambient seismic noise method measures the elastic response of the Earth by extracting the Green Function from the diffuse or random wave fields (Shapiro et al., 2004). It overcomes the difficulties in traditional surface wave measurements such as uneven distribution of seismic

source, the requirement for source information, and the scattering in short periods. The method is becoming an increasingly well-established method to estimate short period (<20 s) and intermediate period (between 20 and 50 s) surface wave speeds on both regional (Sabra et al., 2005; Shapiro et al., 2005; Kang et al., 2006; Yao et al., 2006; Lin et al., 2007) and continental (Bensen et al., 2008; Yang et al., 2007) scales. In these studies, Rayleigh wave Green's Functions between station-pairs are estimated by cross-correlating long time-sequences of ambient noise recorded simultaneously at both stations. The results of these studies showed the Green Functions agree with earthquake records and dispersion curves agree with those measured from earthquakes. Particularly, the resulting tomography maps cohere with known geological structures such as sedimentary basins and mountain ranges (Lin et al., 2008). In addition, the resulting dispersion maps display higher resolution and can obtain much shorter periods than those typically derived from teleseismic earthquakes. Thus the principle purpose of this thesis is to make phase measurements by Rayleigh wave tomography in central and eastern Texas from seismic ambient noise and develop a 3D shear-wave speed model in the crust.

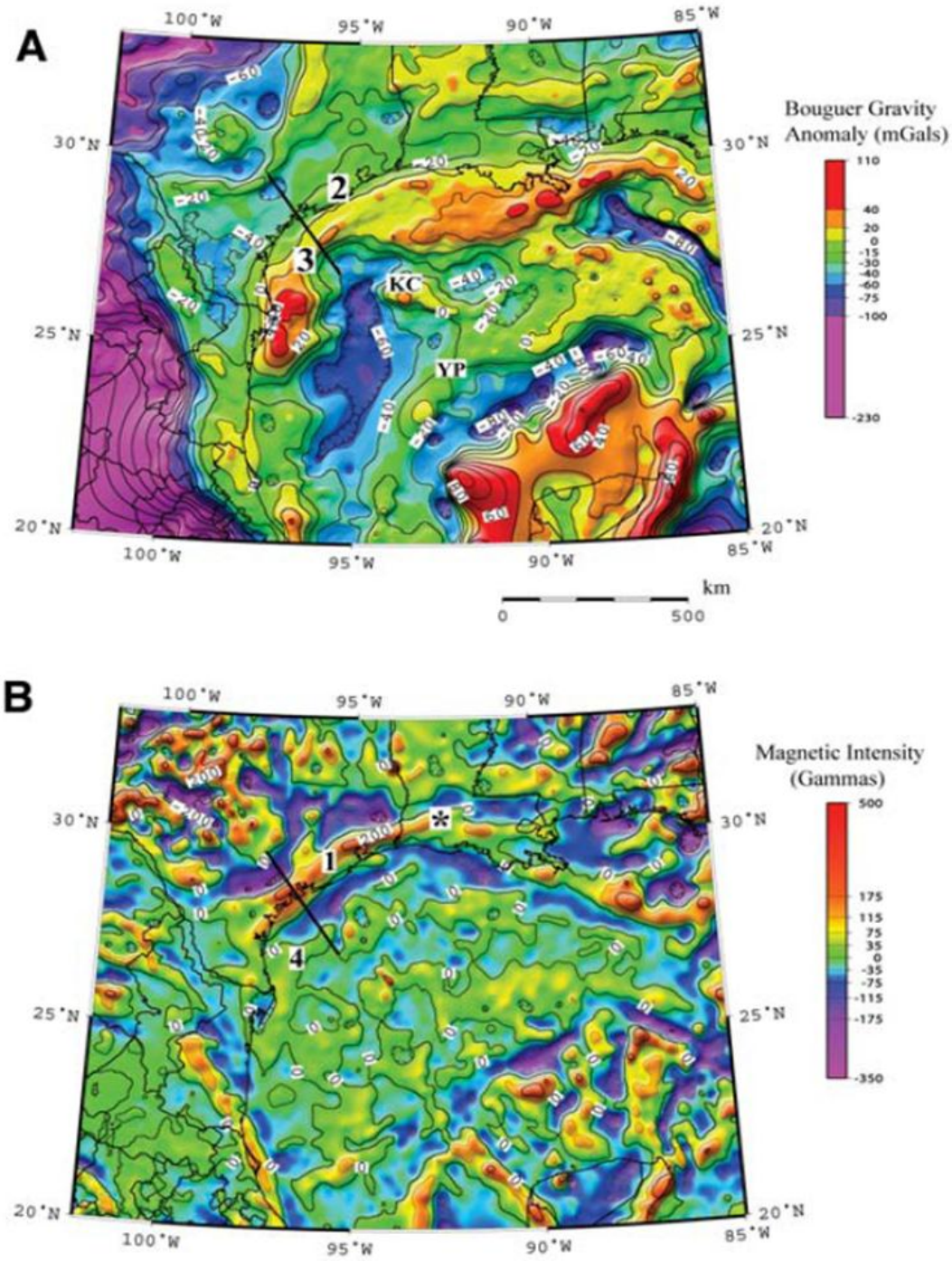

Figure 8- Bouguer gravity anomaly (A) and magnetic intensity map (B) of Texas Coastal Plain and surrounding regions. Contour intervals are 10 mGal and 100 gammas, respectively. Thick line represents location of gravity/magnetic model. (Mickus, 2009)

Gravity and aeromagnetic data in Texas and the Gulf of Mexico were processed to produce Bouguer gravity anomaly and magnetic anomaly maps (Figure 8) (Bankey et al., 2002; Mickus, 2009). The most prominent magnetic anomaly is a large-amplitude maximum that parallels the coastline from Mexico to Lafayette, Louisiana (Figure 8B, anomaly 1). In contrast, the same region on the Bouguer gravity map is characterized by a small-amplitude maximum (Figure 8A, anomaly 2). The high-amplitude magnetic anomaly (Figure 8A, anomaly 1) is 60–80 km wide and has a 300– 400 gammas; it is attributed to a volcanically rifted margin. Besides, in central Texas, there is a high-amplitude magnetic anomaly; the corresponding area in the Bouguer gravity map also has high amplitude compared to surrounding area, which should be the Llano Uplift. There exists a clear boundary between the Llano Uplift and the Coast Plain which extends to northeast direction that should be the Ouachita Mountain Belt.

Rayleigh wave-dispersion experiments carried out by Keller and Shurbet (1975) using different stations in Texas (Corpus Christi, Edinburg, Laredo, San Marcos, and Houston, Figure 9A) show that crustal structure is generally similar along all profiles extending from the Llano Uplift southeastward to the Gulf of Mexico. A generalized crustal structure model proposed by Keller and Shurbet (1975) is shown in Figure 9B. Based on Rayleigh wave-dispersion data, the upper layers (Vp $\leq$5.2 km/s) are interpreted as Mesozoic and Cenozoic sedimentary rocks, the upper crustal layer (Vp >5.2 km/s) is interpreted to consist primarily of Paleozoic metamorphic rocks, and the lower crustal layer (Vp $\leq$6.9 km/s) is interpreted to comprise mafic igneous rocks (Figure 9C). Gravity and refraction data suggest that the lower crustal layer dips to the northwest and that thick Paleozoic sedimentary and meta-sedimentary rocks are present seaward of the buried Ouachita Belt. They indicate that the lower crust is composed of oceanic crust thickened presumably by thrusting and other deformation (Raye et al., 2011).

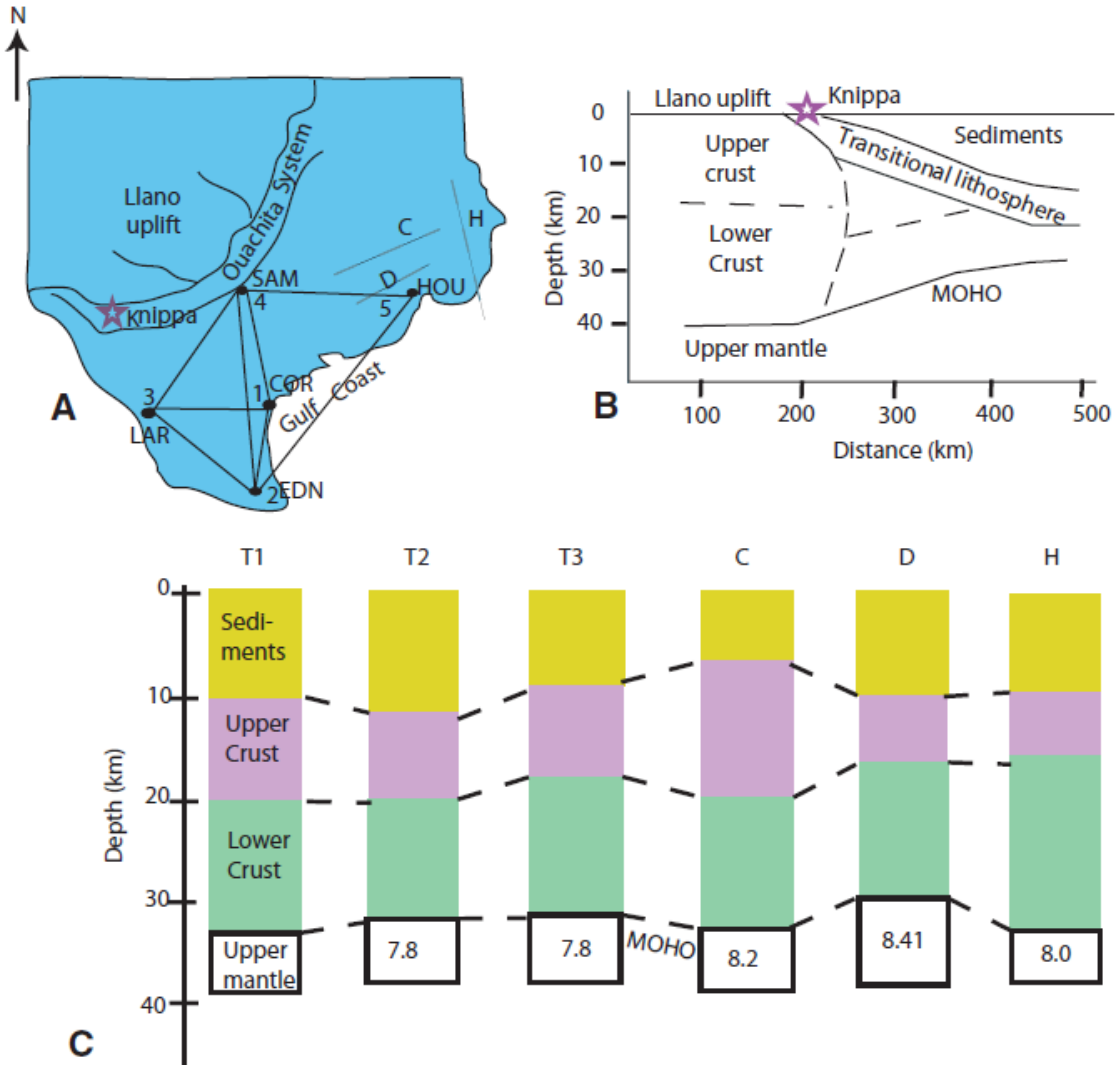

Figure 9- (A) Index map showing Knippa (star), seismograph stations: LAR—Laredo, COR—Corpus Christi, EDN—Edinburg, SAM—San Marcos, HOU—Houston (Keller and Shurbet, 1975), C—Cram (1961, 1962), D—Dorman et al. (1972), H—Hales et al. (1970) refraction line and gravity profiles 1, 2, 3, and 4. T1 (stations 2, 4, and 5), T2 (stations 1, 2, and 3), and T3 (stations 1, 3, and 4) are tripartite locations. (B) Generalized crustal structure model proposed by Keller and Shurbet (1975). (C) Crustal structure as interpreted from seismic velocities. (Raye et al., 2011)

The San Marcos Arch (Figure 10) is prominent north- to northwest-trending basement uplift in the northwestern Gulf of Mexico basin that may be late Mesozoic to Cenozoic foreland or intraplate fold rather than a dome over plutons or buoyant basement blocks. This arch is subparallel to and contemporaneous with orogenic episodes in the northwest-trending fold-thrust belt of Mexico. Arch movement is also contemporaneous with rapid convergence between the North American and Pacific plates. Arch development in the Gulf as a result of tectonic compression is plausible in view of increasing recognition of wide zones of foreland and intraplate deformation in continents. Current tectonic models of the development of the Gulf inaccurately predict gradual, decelerating subsidence when this arch is most active (Stephen et al., 1990). Because of this San Marcos Arch, the basement configuration is showing as Figure 11.

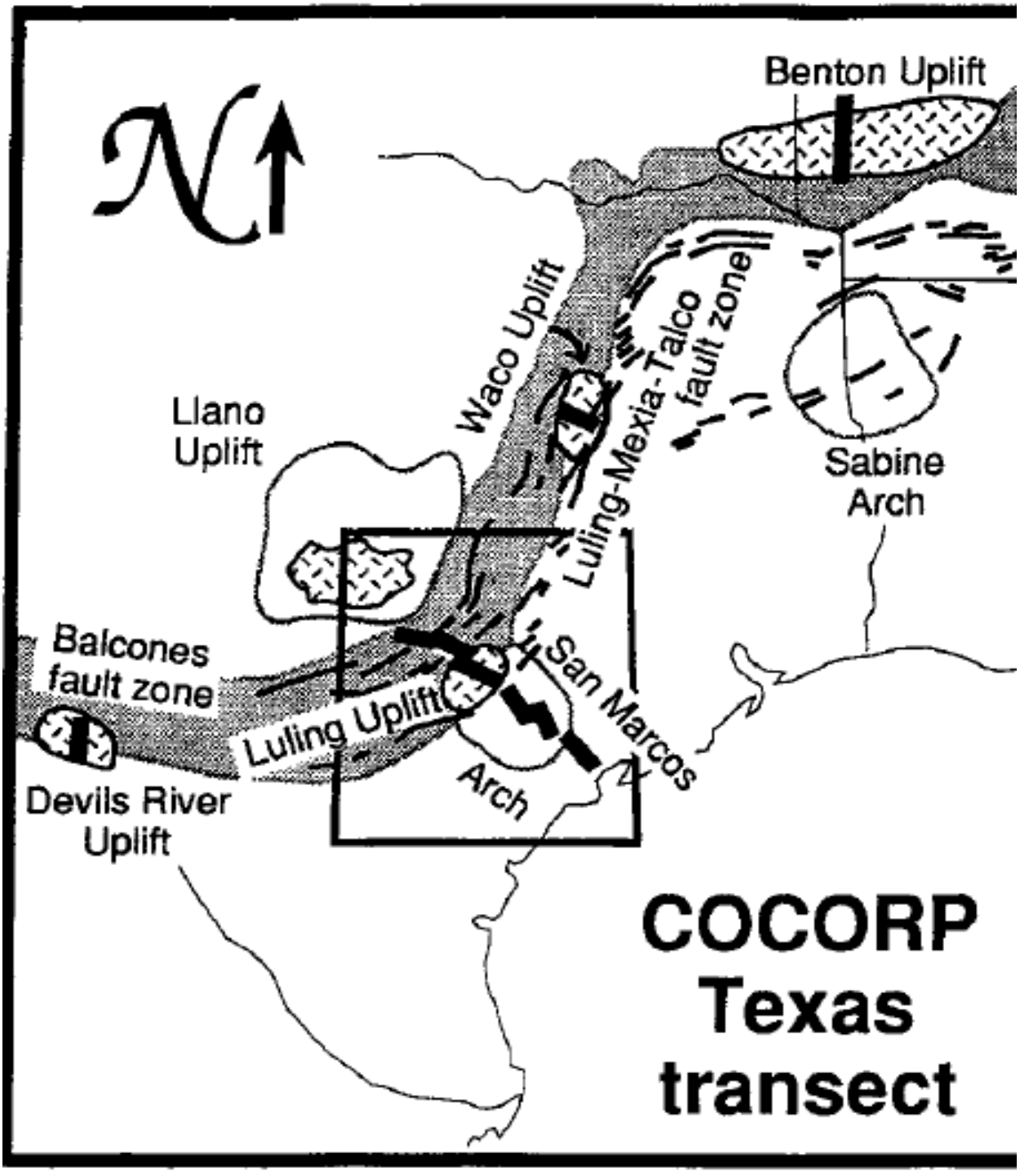

Figure 10– Regional map of Gulf Coast and southern Appalachian-Ouachita orogeny. (Culotta et al., 1992)

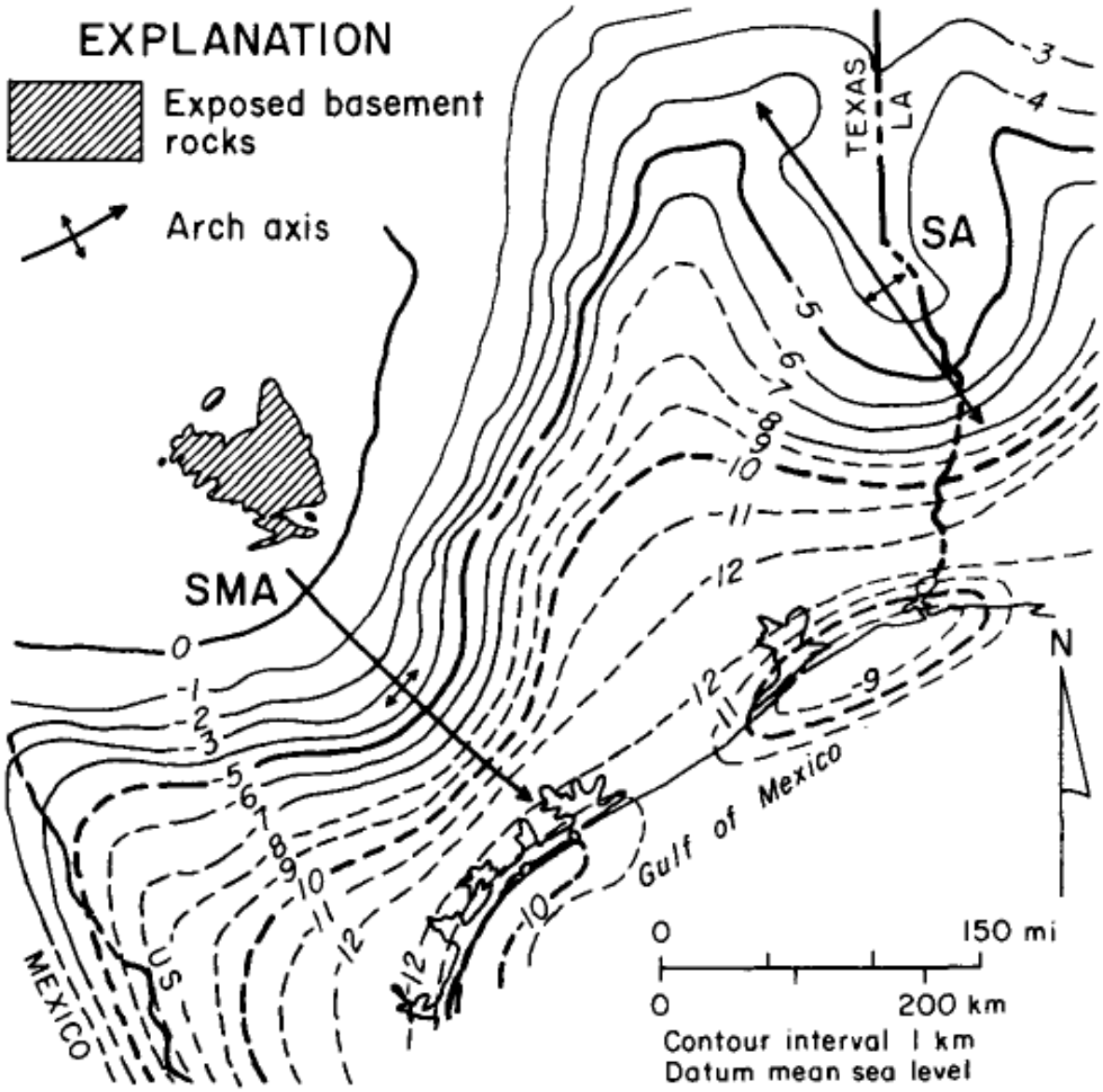

Figure 11- Map showing configuration of basement in northwestern Gulf of Mexico basin based on seismic and well data. (Rosenthal and Buffler, 1987)

3. Data Origin

The seismic data used in this study are from the Transportable Array (TA) stations of USArray, a major component of the NSF EarthScope Project. We chose 87 stations that provided continuous data from March 2010 to February 2011 (Figure 12)**.** Stations of the TA network seismometers are Guralp CMG3T/Quanterra 330 Linear Phase Composite sensors. The ambient noise data are requested at each station by each day. It means the total number of data files is 87 stations multiplied by 365 days, about 30 thousand. We obtaine seismic data from the IRIS (Incorporated Research Institutions for Seismology) Data Management Center via the usual data request tools.

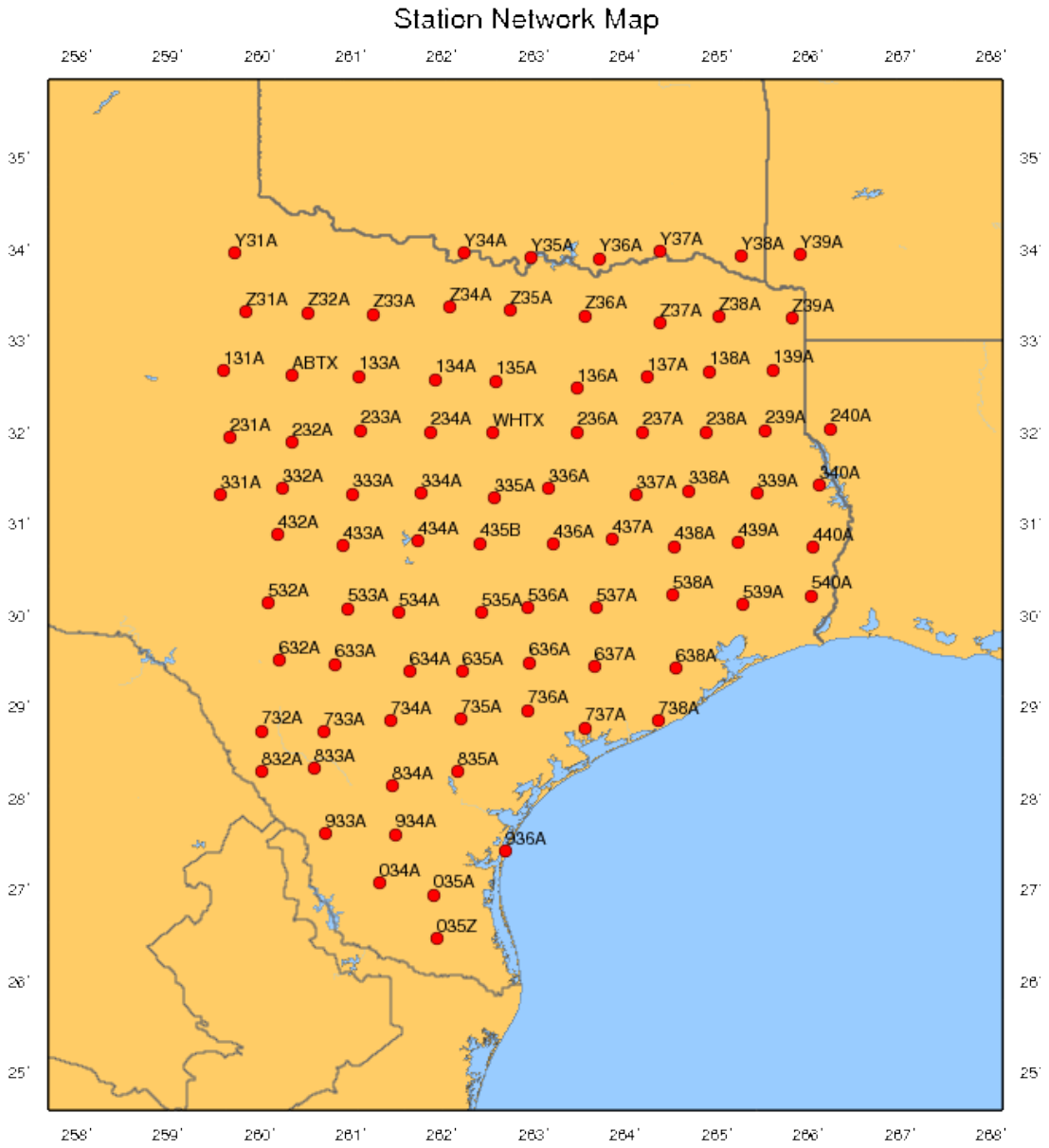

Figure 12- The Map of 87 TA stations for this study

4. Ambient Noise Methodology

Methods used in this study include the ambient seismic noise tomography and the inversion for shear-wave velocity model from phase velocities. This research focuses on processing fundamental mode Rayleigh waves. Rayleigh waves are surface waves that are generated by the interaction of P- and S-waves at the surface of the earth. Rayleigh waves travel with a velocity that is lower than the P-, S-, and Love wave velocities and their amplitude is significant larger than body waves but decreases exponentially with depth. Rayleigh wave phase velocities generally increases with period because fundamental mode Rayleigh waves are primarily sensitive to shear-wave velocity at approximately 1/3 of its wavelength and the speed of shear-waves in the Earth usually increases with increasing depth.

The developments in acoustics (e.g. Weaver and Lobkis, 2001; Derode et al., 2003) and seismology (Campillo and Paul, 2003) suggest an alternative method to measure the elastic response of the Earth by extracting the Green Function from the diffuse or random wave fields. Contrary to ballistic waves (pressure waves), fully diffuse wave fields are composed of waves with random amplitudes and phases but propagating in all possible directions and, therefore, contain the information about any possible path that can be extracted by computing cross-correlations between pairs of receivers.

To demonstrate this property, a modal representation of a diffuse wave field inside an elastic body (Earth) can be expressed as (Weaver and Lobkis, 2001):

$$\emptyset(x,t) = \sum_n a_n u_n(x) e^{i\omega_n t} \quad (1)$$

where x is position, t is time, u_n and ω_n is eigenfunctions and eigenfrequencies of the real Earth, and a_n is modal excitation functions. An important property of the diffuse field is that the modal amplitudes are uncorrelated random variables:

$$< a_n a_m^* >= \delta_{nm} F(\omega_n) \quad (2)$$

where F(ω) is the spectral energy density. Because the cross-correlation between the fields at locations x and y becomes simply:

$$C(x, y, \tau) = \sum_n F(\omega_n) u_n(x)\, u_n(y) e^{-i\omega_n \tau} \quad (3)$$

The expression equation (3) differs only by an amplitude factor F from an actual Green function between points x and y. It is an important implication that the Green's function between two locations can be extracted from the diffuse field with a simple field-to-field correlation taken over sufficiently long time. This is the fundamental theory of the Ambient Noise Tomography. Ambient Noise Tomography has been widely applied to many places such as in California and the Pacific Northwest (Moschetti et al., 2007) and in Tibet (Yao et al., 2006). However, most of the earlier studies, like the work of Shapiro et al. (2005), have been performed in the microseism frequency band below 20 s to obtain group velocities. Bensen et al. (2005 and 2007) extended the method to considerably longer periods and phase velocity calculation. The detail procedures of data processing that underlie ambient noise tomography were summarized by Bensen et al. in 2007. The ambient noise processing procedures applied here is basically the same as the one described by Bensen et al. (2007). We use only the vertical component of ambient noise data which means that the cross-correlations provide only Rayleigh wave signals. The concrete steps for data processing scheme are shown in Figure 13.

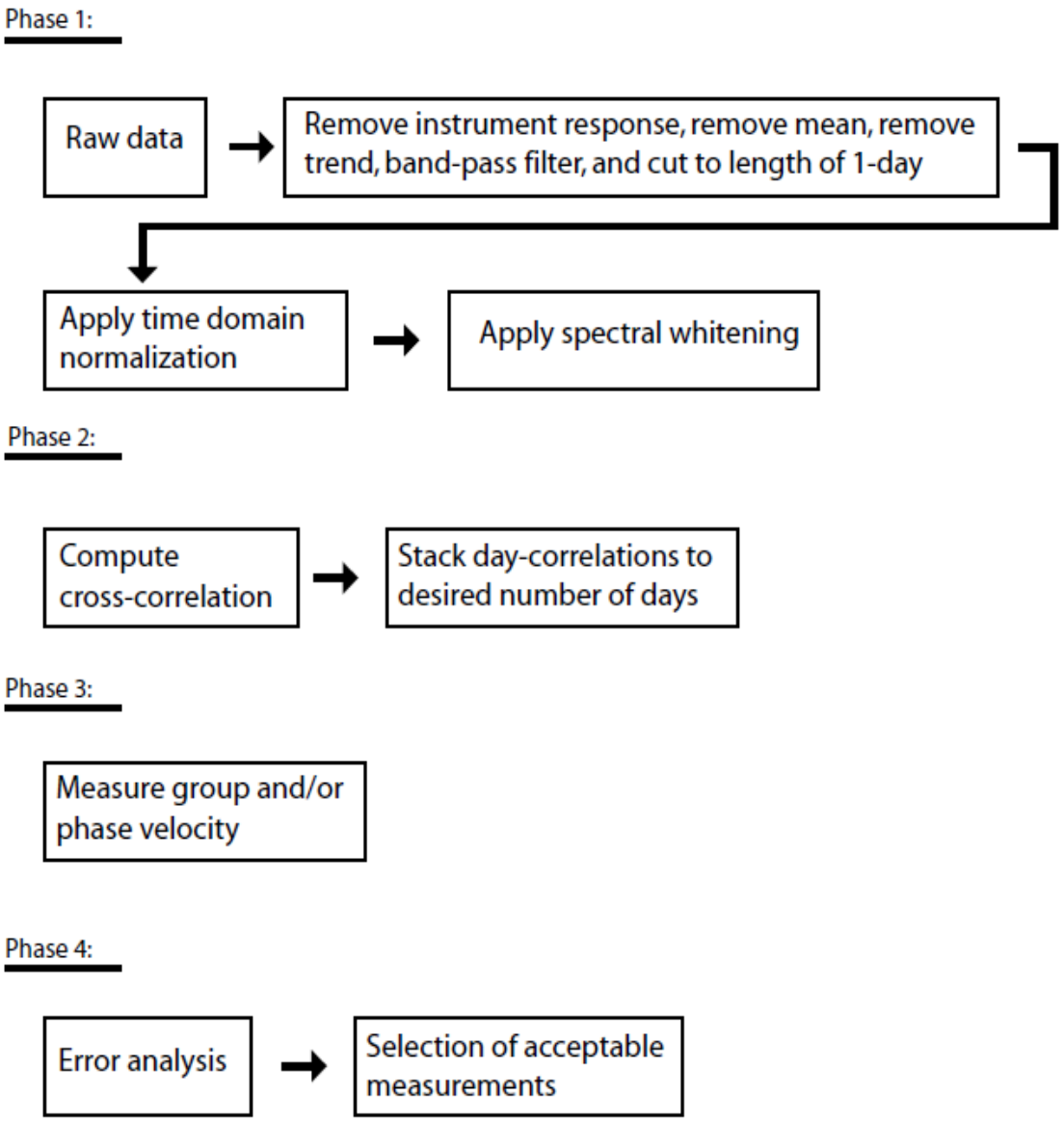

Figure 13- Schematic representation of Ambient Seismic Noise processing steps. (Bensen et al., 2007)

5. Ambient Noise Data Processing

5.1 Single Station Data Preparation:

The first phase of data processing consists of preparing waveform data from each station individually. The purpose of this phase is to accentuate broad-band ambient noise by attempting to remove earthquake signals and instrumental irregularities that tend to obscure ambient noise. It contains temporal normalization and spectral normalization or whitening**.** In this study, daily waveforms at each station are filtered in a broad band of period from 5 s to 50 s. Spectral whitening is an important step, which broadens the band of the ambient noise signal in cross-correlations and also combats degradation caused by persistent monochromatic source spectral normalization.

We requeste the seismic data for every day through March 1st 2010 to February 28st 2011 from IRIS website for the following stations:

Network	Name	Lon.	Lat.		Network	Name	Lon.	Lat.
TA	034A	-98.68	27.06		TA	538A	-95.49	30.22
TA	035A	-98.1	26.94		TA	539A	-94.72	30.11
TA	035Z	-98.07	26.46		TA	540A	-93.98	30.21
TA	131A	-100.39	32.67		TA	632A	-99.79	29.51
TA	133A	-98.92	32.61		TA	633A	-99.18	29.46
TA	134A	-98.08	32.57		TA	634A	-98.35	29.38
TA	135A	-97.41	32.56		TA	635A	-97.77	29.39
TA	136A	-96.53	32.47		TA	636A	-97.06	29.48
TA	137A	-95.76	32.6		TA	637A	-96.33	29.44
TA	138A	-95.09	32.66		TA	732A	-99.97	28.73
TA	139A	-94.39	32.68		TA	733A	-99.29	28.72
TA	231A	-100.32	31.94		TA	734A	-98.56	28.85
TA	232A	-99.65	31.89		TA	735A	-97.81	28.86
TA	233A	-98.9	32.02		TA	736A	-97.07	28.95
TA	234A	-98.14	32		TA	737A	-96.44	28.76
TA	236A	-96.53	32		TA	738A	-95.65	28.84
TA	237A	-95.81	32		TA	832A	-99.97	28.28
TA	238A	-95.12	32		TA	833A	-99.39	28.32
TA	239A	-94.47	32.02		TA	834A	-98.55	28.13
TA	331A	-100.43	31.31		TA	835A	-97.83	28.29
TA	332A	-99.74	31.38		TA	933A	-99.27	27.61
TA	333A	-98.98	31.32		TA	934A	-98.52	27.6
TA	334A	-98.24	31.33		TA	936A	-97.31	27.42
TA	335A	-97.43	31.28		TA	ABTX	-99.64	32.62
TA	336A	-96.84	31.39		TA	WHTX	-97.46	31.99
TA	337A	-95.89	31.32		TA	Y31A	-100.26	33.96
TA	338A	-95.31	31.36		TA	Y32A	-99.44	34
TA	339A	-94.56	31.33		TA	Y33A	-98.63	34.01
TA	340A	-93.89	31.42		TA	Y34A	-97.76	33.96
TA	432A	-99.79	30.88		TA	Y35A	-97.04	33.91
TA	433A	-99.09	30.75		TA	Y36A	-96.28	33.9
TA	434A	-98.27	30.81		TA	Y37A	-95.62	33.98
TA	435B	-97.58	30.78		TA	Y38A	-94.73	33.93
TA	436A	-96.8	30.77		TA	Y39A	-94.09	33.94
TA	437A	-96.14	30.83		TA	Z31A	-100.14	33.32
TA	438A	-95.47	30.75		TA	Z32A	-99.48	33.31
TA	439A	-94.77	30.79		TA	Z33A	-98.76	33.29
TA	440A	-93.96	30.75		TA	Z34A	-97.92	33.37
TA	532A	-99.9	30.13		TA	Z35A	-97.25	33.33
TA	533A	-99.04	30.07		TA	Z36A	-96.43	33.27
TA	534A	-98.48	30.03		TA	Z37A	-95.62	33.2
TA	535A	-97.57	30.03		TA	Z38A	-94.99	33.26
TA	536A	-97.07	30.08		TA	Z39A	-94.18	33.24

- Table 1- The name, longitude and latitude of 87 TA stations for this study.

Firstly, we prepare single station data preparation for every station every day (Figure 14). Then we make cross-correlations for between to every possible pair of stations for one-day data and stack them for one-month time interval**.** Then we stack every month data to form one year in order to increase signal-to-noise ratio (Figure 15). And since each cross-correlated waveform is separated into positive and negative components, we add the two components to create a final cross-correlation as shown Figure 16. The subsequent data processing phases are applied only on these "symmetric" cross-correlated waveforms. With these final cross-correlation results, we calculate the phase velocity for different periods between every pair of the stations to make phase velocity tomography maps.

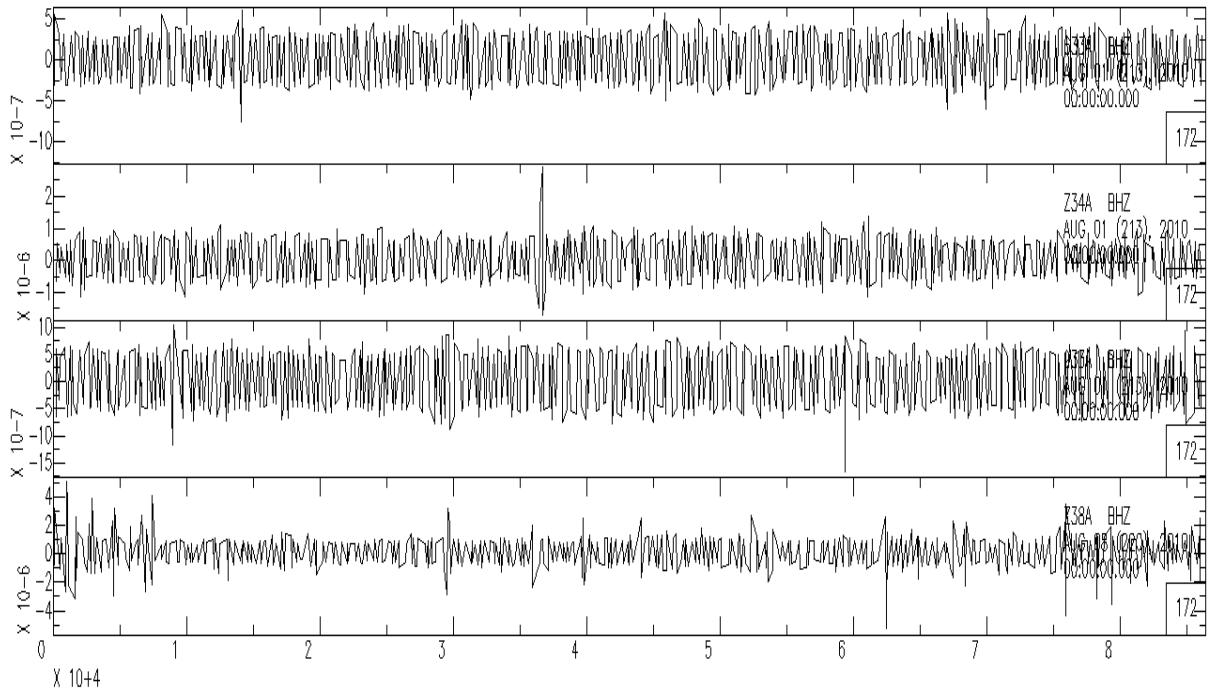

Figure 14- Waveforms displaying examples after single station preparation for 633A, 933A, Z34A, and Z38A stations with data on August, 1, 2010.

5.2 Cross-correlation and Stacking

After preparation of the daily time-series, the next step in the data processing scheme is cross-correlation and stacking. Although some interstation distances may be either too short or too long to obtain reliable measurements, we just need to perform cross-correlations between all possible station pairs at this stage and data selection is performed at a later phase.

Cross-correlation is performed daily in the frequency domain. After the daily cross-correlations are returned to the time domain they are added to one another, or 'stacked', to correspond to longer time-series. Alternately, stacking can be done in the frequency domain which would save the inverse transform (Figure 15).

The use of long time-series helps to optimize the signal-to-noise ratio (SNR), which negatively correlated with measurement error. Rayleigh wave trains are clearly emerged on all traces and the signals are largely symmetric on both positive and negative lags.

In order to increase signal-to-noise ratio, each cross-correlated waveform is separated into positive and negative components and the two components are added to create a final "symmetric" cross-correlation. The subsequent data processing phases are applied only on these "symmetric" cross-correlated waveforms (Figure 16).

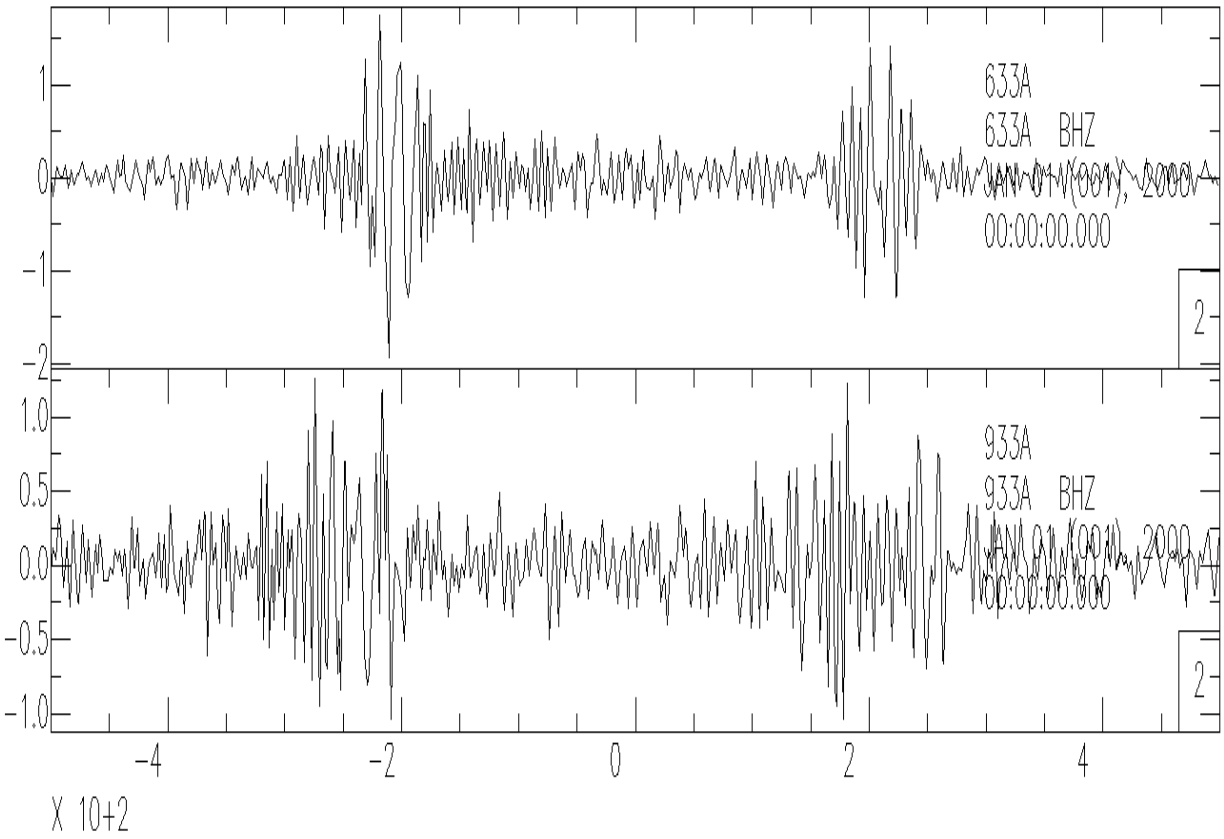

Figure 15 – Cross-correlation stacking results for data of one year between station 633A to station Z34A and station 933A to station Z38A.

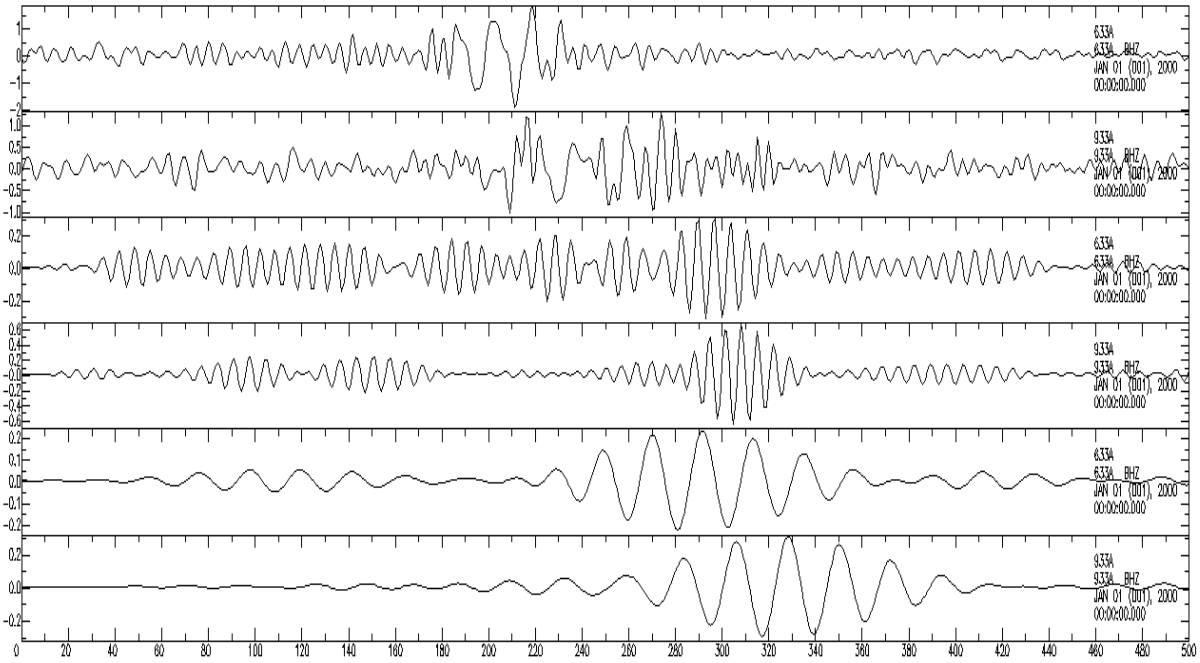

Figure 16 – Example of a broad-band symmetric-component cross-correlation between station 633A to Z34A and station 933A to Z38A of the TA network in East Texas. The broad-band signal (5 to 50 s) is shown at top, the 6 to 8 second is presented in the two middle figures and the 20 to 25 second is presented at bottom. (The symmetric component is the average of the cross-correlation at positive and negative lags.)

6. Dispersion Measurements

After the daily cross-correlations have been computed and stacked, the resulting waveform is an estimated Green function. Using the estimated Green function, the group and phase speeds as a function of period can be measured by using traditional frequency-time analysis (FTAN) (Figure 17) (e.g. Dziewonski et al., 1969; Levshin and Ritzwoller, 2011).

And phase slowness can be derived from group velocity from a vertical component ambient noise cross-correlation (Bensen et al, 2007):

$$S_c = S_u + (\omega\Delta)^{-1}\left(\emptyset(t_u) + 2\pi N - \frac{\pi}{4}\right) \qquad (4)$$

where N=0, $\pm 1, \pm 2, \ldots$, S_c and S_u are phase and group slowness, ω is frequency, Δ is interstation distance, $\emptyset(t_u)$ is the observed phase at the observed group arrival time, $t_u = \Delta/U$, U is group speed.

Rayleigh wave phase velocity variations in this study are obtained at periods of 6, 8, 10, 12, 14, 16, 18, 20, 25, 30, 35, and 40 s. Compare to group velocity, the uncertainty of phase velocity measurements is smaller and phase velocity also has a greater sensitivity for deeper structures.

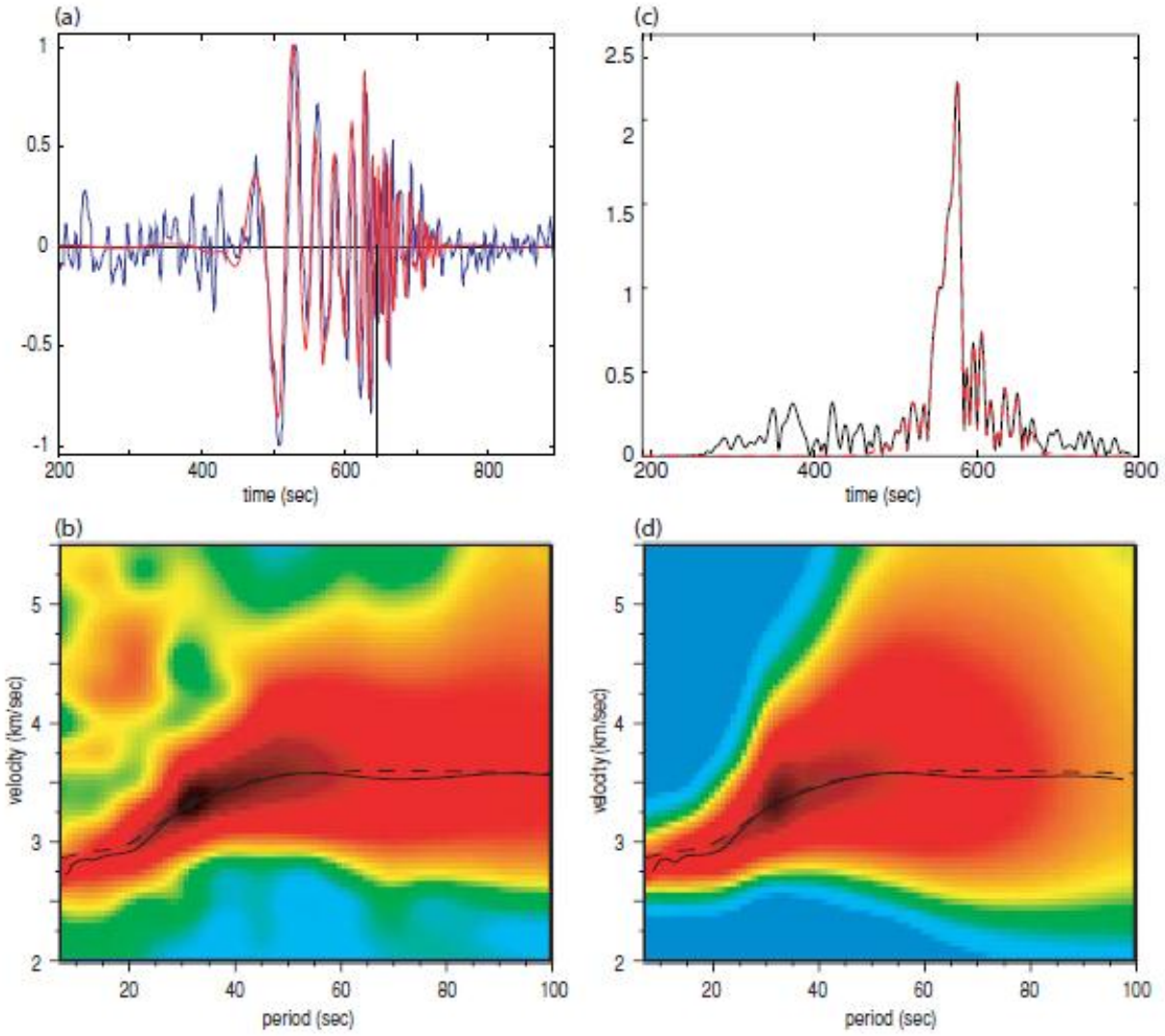

Figure 17- Graphical representation of FTAN. (a) Raw (blue) and cleaned (red) waveforms for the 12-month stacked cross-correlation between stations ANMO and COR (Corvallis, OR, USA). (b) Raw FTAN diagram, measured group speed curve as the solid line and prediction from the 3-D model of Shapiro and Ritzwoller (2002) as the dashed line. (c) Undispersed or collapsed signal (black) and cleaned signal (red dashed). (d) Cleaned FTAN diagram, measured group speed curve and prediction from the 3-D model of Shapiro and Ritzwoller (2002). (Bensen et al., 2007)

Following descriptions above, phase velocities at all possible station pairs are calculated. For example, we choose four stations in our study: 633A and Z34A are located in the Laurentia Craton area while 933A and Z38A are located in Gulf Coast (Figure 18). The phase velocity between this two station pairs show a large difference despite their same direction and close location (Figure 19). The blue, green, and red line separately show phase velocity between 633A to Z34A, average phase velocity of whole study area and phase velocity between 933A to Z38A. The largest difference of phase velocity between two station pairs is from 6 s to 10 s period which represented the sediment and top crust area. From 10 s to 25 s periods, the difference becomes small with the depth from middle crust to lower crust. In the lower crust and upper mantle, from 25 s to 40 s periods, the phase velocity between this two station pairs change to almost same.

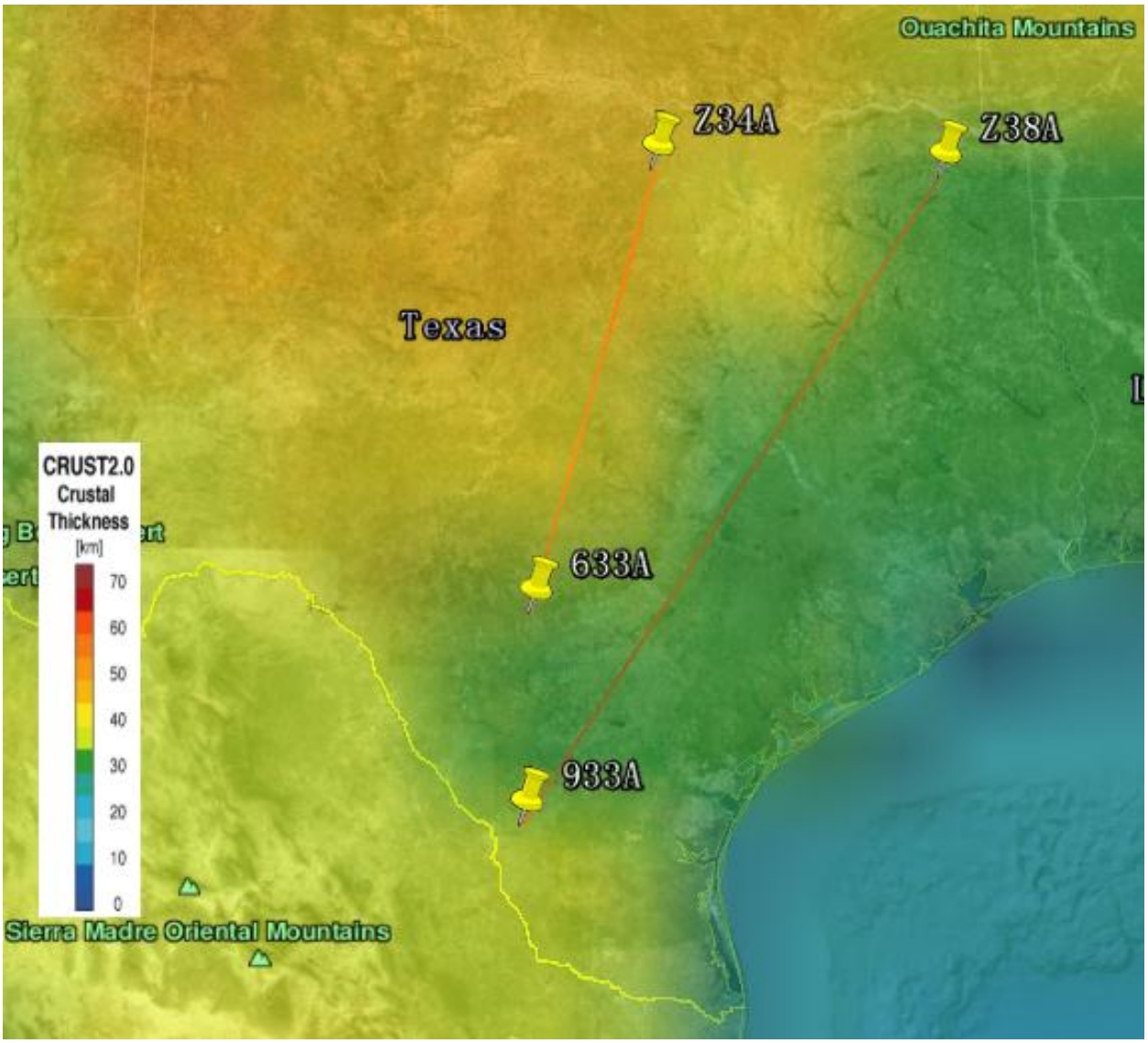

Figure 18– Crust thickness distribution in Texas from Crust 2.0 Model. 633A, Z34A, 933A and Z38A are four stations chosen from 87 stations in our study. 633A and Z34A are located in Laurentia Craton area while 933A and Z38A are located in Gulf Coast.

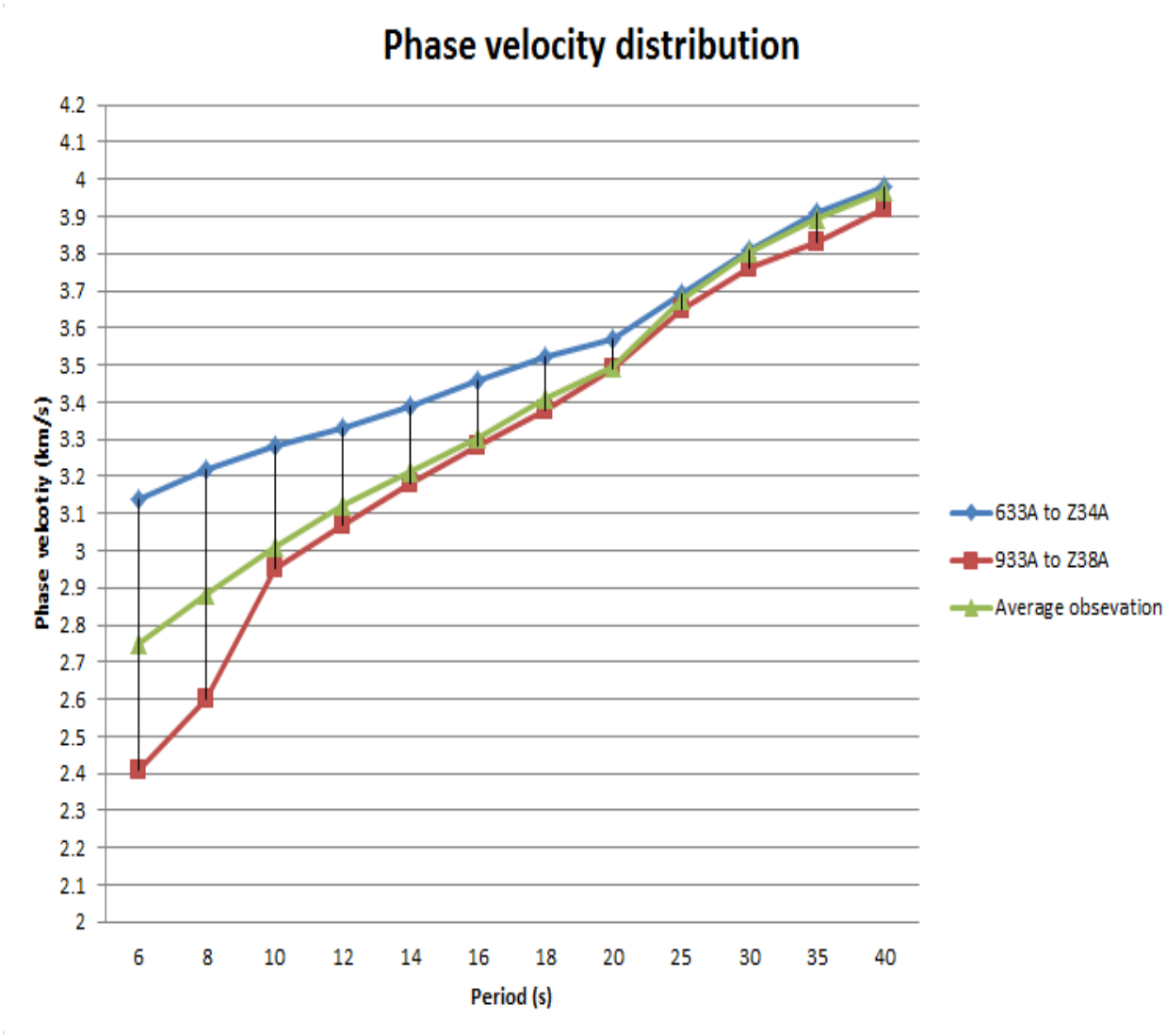

Figure 19 – Comparison of absolute phase velocity of two pairs of stations and average observation.

7. Ambient Noise Tomography

After dispersions are obtained at all possible station pairs, the next step is to use these dispersions to develop 2D phase velocity maps. Considered the quality control, we draw the ray path of phase velocity tomography results for 6 to 40 s periods (Figure 20 and 21). Because the number of interstation paths grows as n*(n-1)/2 times of stations where n is station number. The data processing procedure that is applied to ambient noise cross-correlations has been designed to require minimal human interaction. The signal/noise ratio is an important parameter used to reject bad measurements. To reject low quality data and ensure reasonable ray paths for tomography, an SNR of 20 is used as threshold for acceptable waveforms between 6 s to 25 s periods and an SNR of 10 is used for waveforms between 25 s to 40 s. When an SNR of 20 is used as threshold, the numbers of ray path for different periods are: 332 for 6 s, 3852 for 8 s, 4130 for 10 s, 4206 for 12 s, 4906 for 14 s, 5274 for 16 s, 5304 for 18 s, 5060 for 20 s, 3744 for 25 s, 2266 30 s, 1196 for 35 s, and 298 for 40 s. We notice that the number of ray path increasing from 6 s to 18 s and decreasing from 18s to 40s, so the best resolution is at 18 seconds period. An important criterion applied in selecting phase velocity measurements for the tomography is that the distance between the station pair is greater than 3 times of the wavelength. This leads to that the number of rays decreases with increasing period. For avoided this decreasing, a SNR 10 is used to obtain numbers of ray path: 5930 for 25 s, 4910 for 30 s, 3726 for 35 s, and 1420 for 40s. At all periods, we could expect high resolution on whole central Texas. Only the northeastern part of Gulf Coast might not be well resolved at longer periods than 25 seconds.

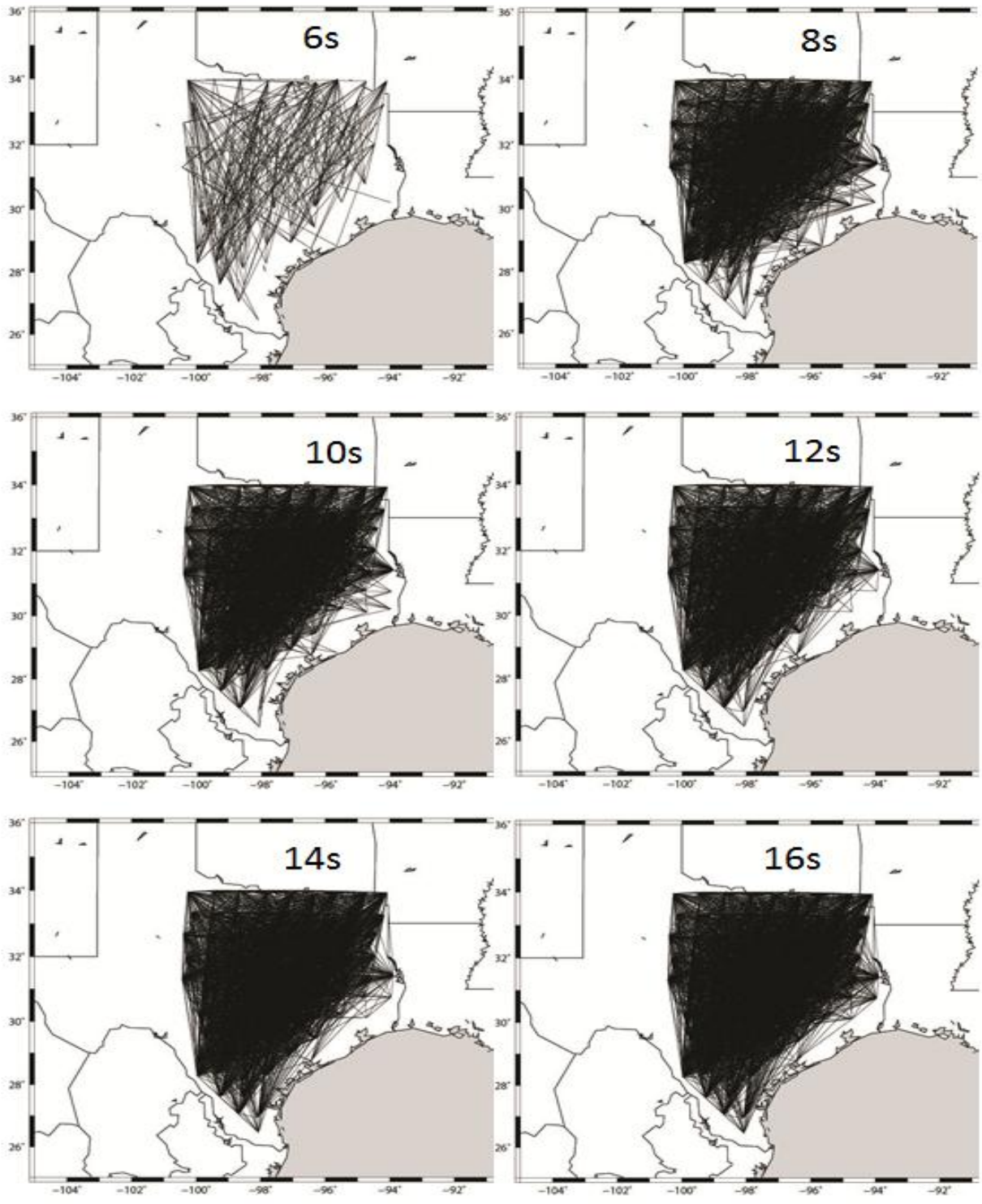

Figure 20 – Ray path for Rayleigh wave phase velocity anomaly maps in period of 6, 8, 10, 12, 14 and 16 seconds (with S/N ratio 20).

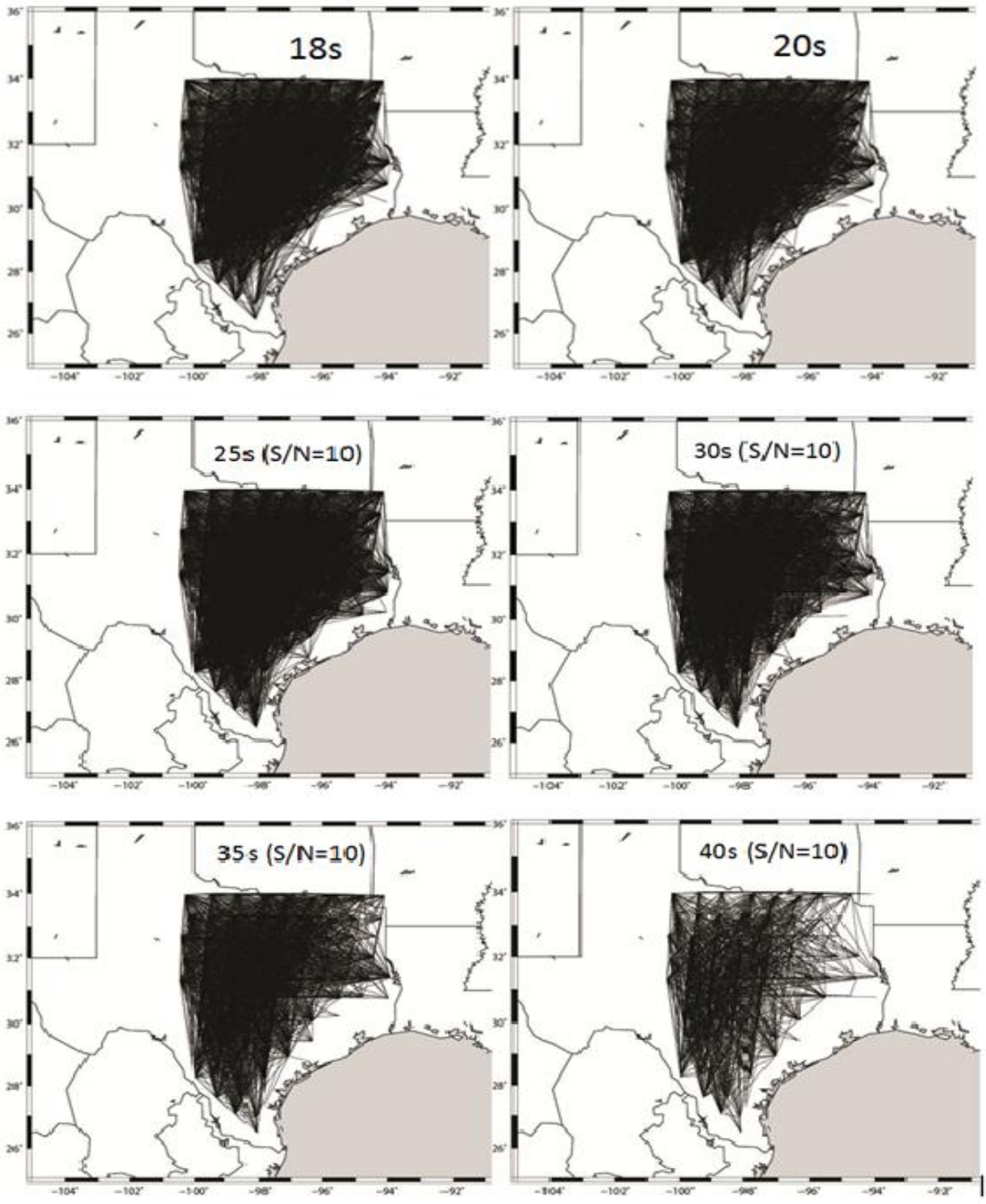

Figure 21 – Ray path for Rayleigh wave phase velocity anomaly maps in period of 18, 20, 25 seconds (with S/N ration 20) and 30, 35, 40 seconds (with S/N ratio 10)

The Rayleigh wave phase velocity measurements at all station pairs are inverted for 2D phase velocity maps on a grid of 0.5^o by 0.5^o using the method of Barmin et al. (2001). This method is based on minimizing a penalty function composed of a linear combination of data misfit, model smoothness and the perturbation to a reference model for isotropic wave speed (Yang et al., 2007). Phase velocities at each period from 6 s to 40 s are determined at all grid nodes. The average phase velocities in the entire study area are calculated based on 2D data for all periods (Figure 22) and these values are used as reference to calculate phase velocity perturbations in Figure 23.

The features of the maps vary with period because of the different sensitivity depths of Rayleigh waves at different periods. For fundamental mode Rayleigh wave, it has the highest sensitivity at 1/3 of its wavelength. Maps of short periods (6 to 10 s) are mainly sensitive to shear-wave velocities in the upper crust. Maps of mid-periods (10 to 25 s) are sensitive to shear-wave velocity in the mid-crust. And the maps of long periods (25 to 40 s) are more sensitive to crustal thickness and shear-wave velocities in the lower crust to uppermost mantle.

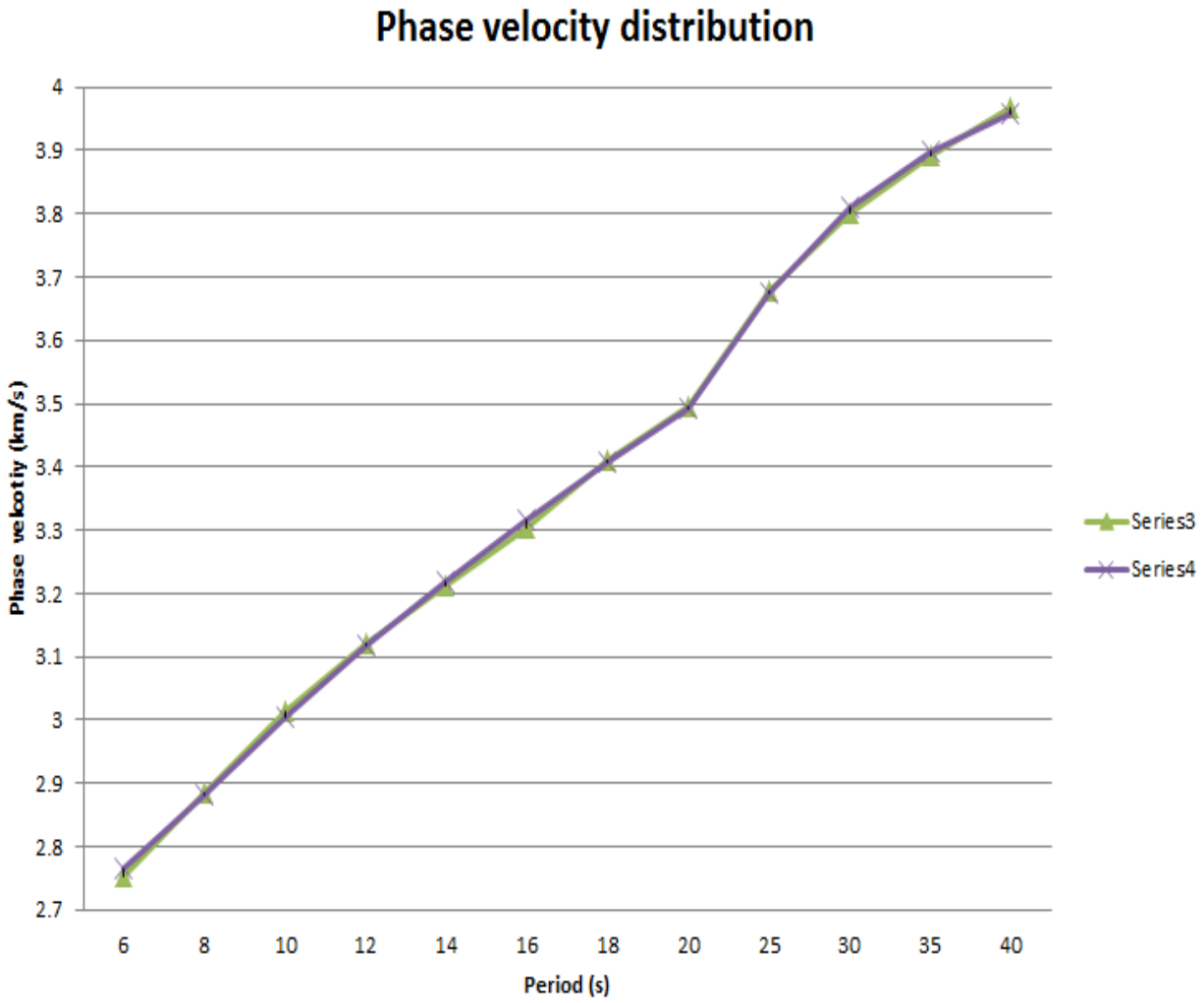

Figure 22– Average and predicted phase velocities. The green line is average phase velocities while the purple line is predicted phase velocities by 1-D inversion model.

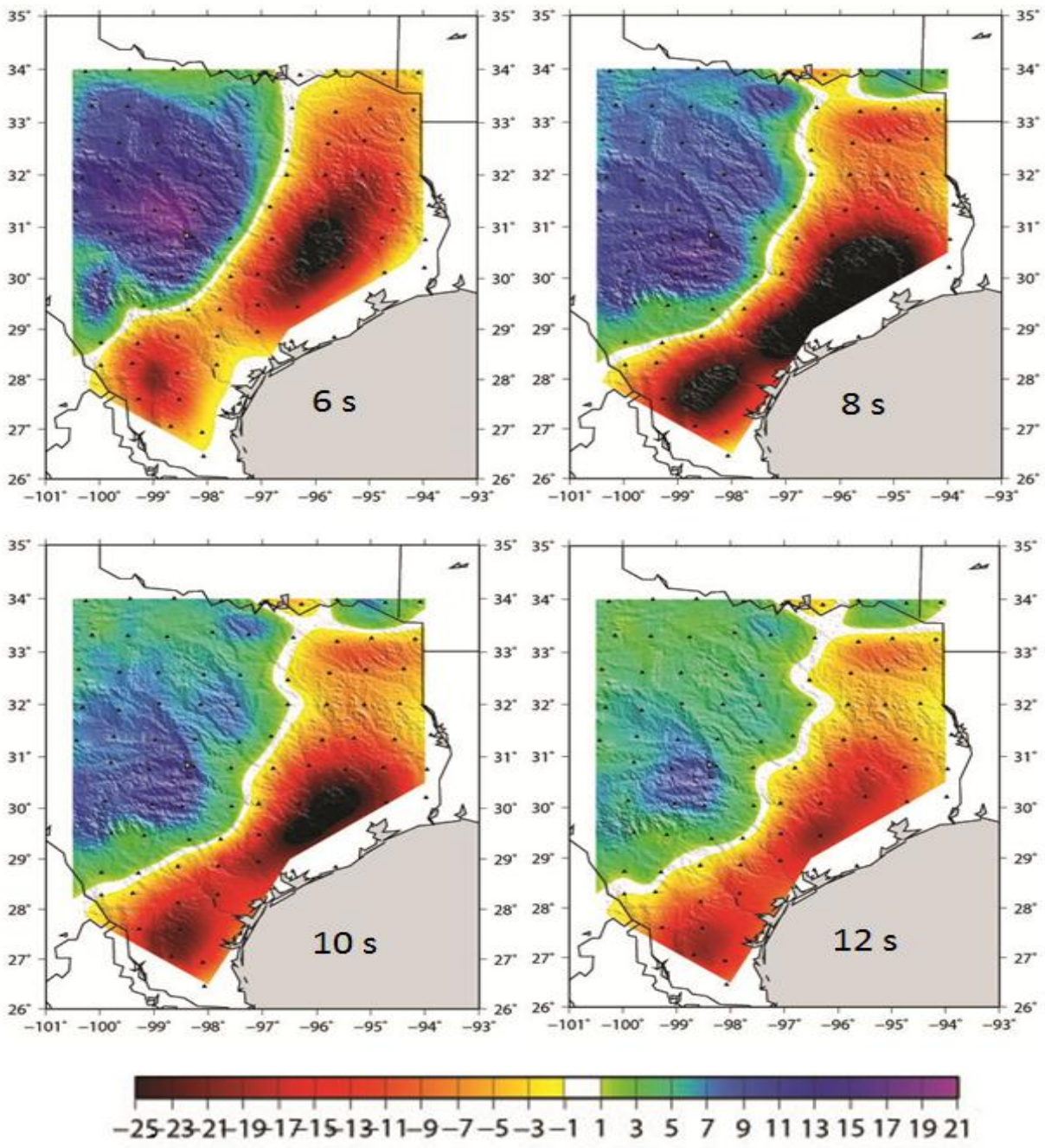

Figure 23(1) – Phase velocity anomaly tomography maps from Ambient Seismic Noise data using the TA stations data in central and eastern Texas of periods 6, 8, 10, and 12 seconds. These are velocity anomaly maps and they illustrate the percentage velocity anomaly compared to local average velocities. And the different color scale is shown under each picture.

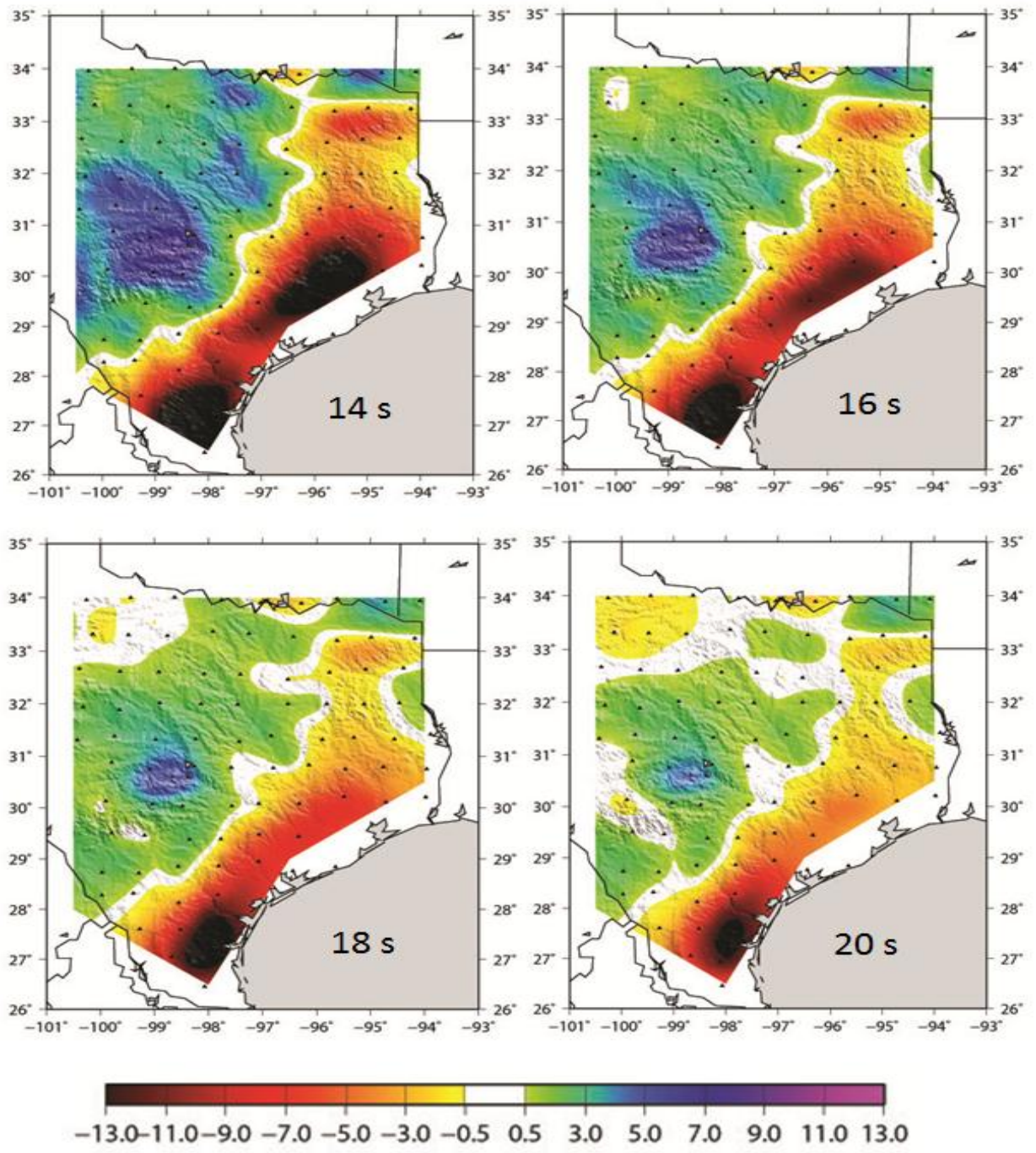

Figure 23(2) – Phase velocity anomaly tomography maps from Ambient Seismic Noise data using the TA stations data in central and eastern Texas of periods 14, 16, 18, and 20 seconds. These are velocity anomaly maps and they illustrate the percentage velocity anomaly compared to local average velocities. And the different color scale is shown under each picture.

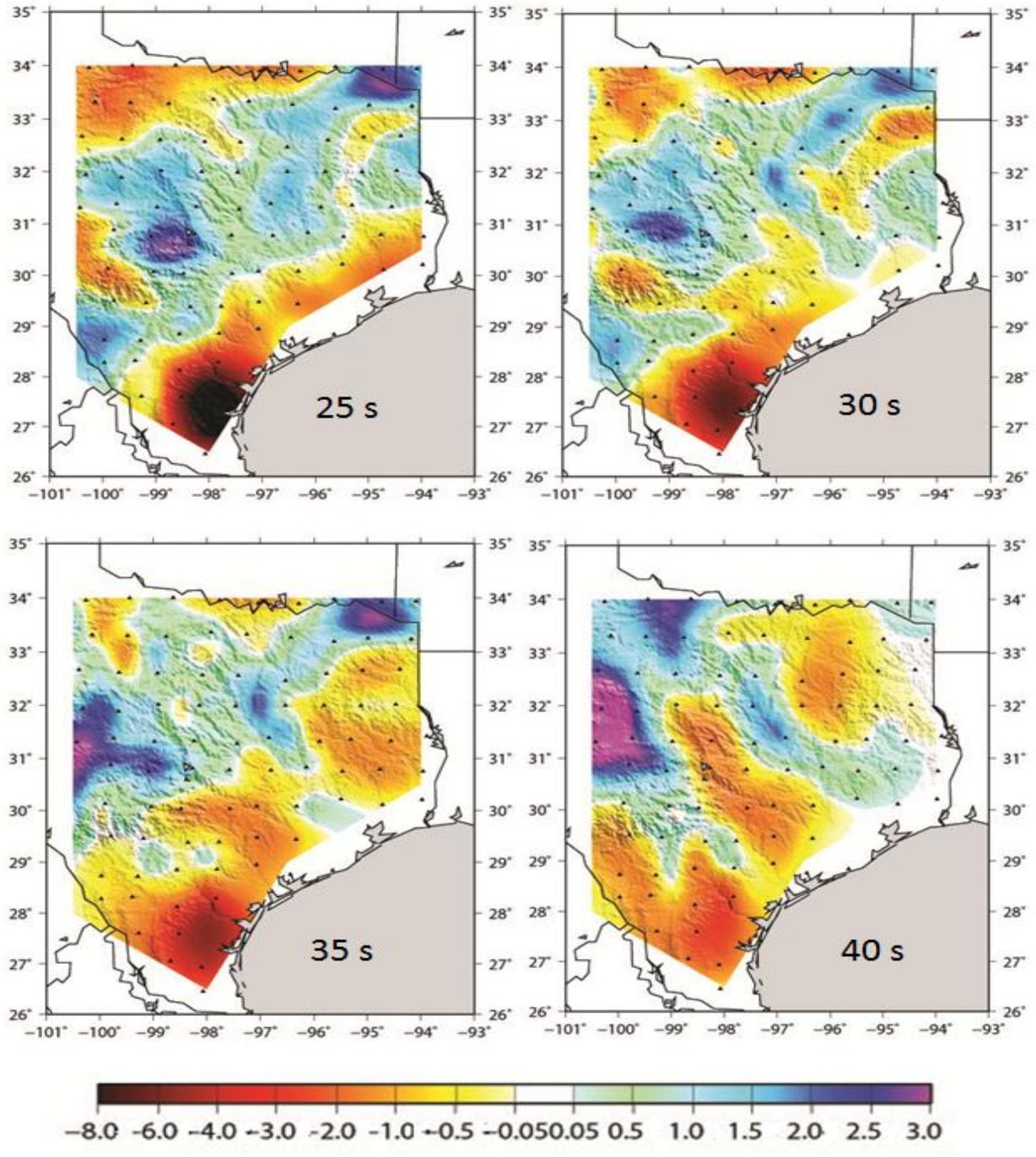

Figure 23(3) – Phase velocity anomaly tomography maps from Ambient Seismic Noise data using the TA stations data in central and eastern Texas of periods 25, 30, 35, and 40 seconds. These are velocity anomaly maps and they illustrate the percentage velocity anomaly compared to local average velocities. And the different color scale is shown under each picture.

The phase velocity anomaly maps show clear difference between the central Texas in northwest and the coast of Gulf Mexico in southeast. In the period range of 6 to 25 s, all the maps are similar with positive anomaly corresponding with the stable craton area in the central Texas and the negative anomaly area coincides with the coast plain along the continental margin. The boundary between these two different parts perfectly correlates to the Ouachita Belt, which is the boundary separated the Laurentia craton and the rifted continental margin. The degree of phase velocity anomaly decreases with increasing period, which could be seen by the reduced color-scale at longer periods.

The place of highest phase velocity is located right at the Llano Uplift at all periods. The lowest phase velocity is imaged in eastern Texas Basin from 6 to 16 s and in southeastern continental margin at all periods. The distribution of phase velocity anomaly from periods above 20 s shows a different pattern from that at shorter periods. At periods of 25 to 30 s, small patches of high-velocity anomaly also show up at the Texas-Mexico boarder and northeastern Texas. The negative phase velocity anomaly is not ubiquitous along the coast of the Gulf Mexico but appears as broken patches and becomes oriented in NW-SE directions.

8. Shear-wave Velocity Model

The 1-D shear-wave model of the central and eastern Texas is obtained by using the average phase velocities (Figure 22) at a period range of 6 to 40 s determined from the ambient noise data. The model parameters of this inversion are shear-wave velocities in 12 layers from the Earth's surface to 200 km depth with different layer thicknesses. We modify the AK135 (Kennett et al., 1995) to form the starting model for the inversion and changed the original three-layer crust to four layers to account for variation of sediment thickness in the area. The top two layers are 5 kilometers thick, respectively. The third layer is 10 km thick and the fourth layer is 20 km thick. Layer thickness in the mantle is 20 km. P- and S-wave velocities and densities in the initial model are from the AK135 model.

Since the relation between shear-wave speeds and phase velocities is non-linear, we have linearized this relation and performed an iterative search for the optimal solution. The method of Saito (1988) is used to compute the synthetic phase velocities and partial derivatives with respect to changes in P-wave and S-wave speeds. We choose 0.05km/s as a priori error for the model parameters, shear-wave velocities in each layer, which can fit the data and keep the model smooth.

In order to build a 3-D shear-wave model from the calculated 2D phase velocities from the ambient seismic noise tomography, we use the 1-D shear-wave velocity as the initial model. And we choose the Crust 2.0 model (Bassin et al., 2000) as a priori constraint to the crust thickness at each grid point. The general trend we could find that the crust thickness became thinner from

northwestern to southeastern in our study area. The 3D model is constructed by assembling the 1-D shear-wave models at each point of the 0.5^{o} by 0.5^{o} grid.

Given that the longest period from the ambient noise tomography is 40 s with an average phase velocity of 3.96 km/s, its highest sensitivity is 54km. We therefore focus on shear-wave velocity results in the top five layers that contain four crust layers and one uppermost mantle layer up to 60 km depth.

The 1-D shear-wave model of the study area is shown in Figure 24B, which does a good job in fitting the observed phase velocities (Figure 22A). Compared with the starting AK135 model, which has 3.46 km /s for the top two layers, the average shear-wave in the up curst (0-10 km) in the central and eastern Texas is extremely slow with a value of 2.8 km/s and 2.9 km/s, respectively. Such a slow upper crust is largely due to the thick sediment layers in the coast plain. In AK135 model, the shear-wave velocity for third, fourth, and fifth layer is 3.46, 3.85, and 4.48 km/s. And in 1-D inversion result, the corresponding velocity is 3.44, 3.89, and 4.59 km/s which don’t have much difference from the AK135 model.

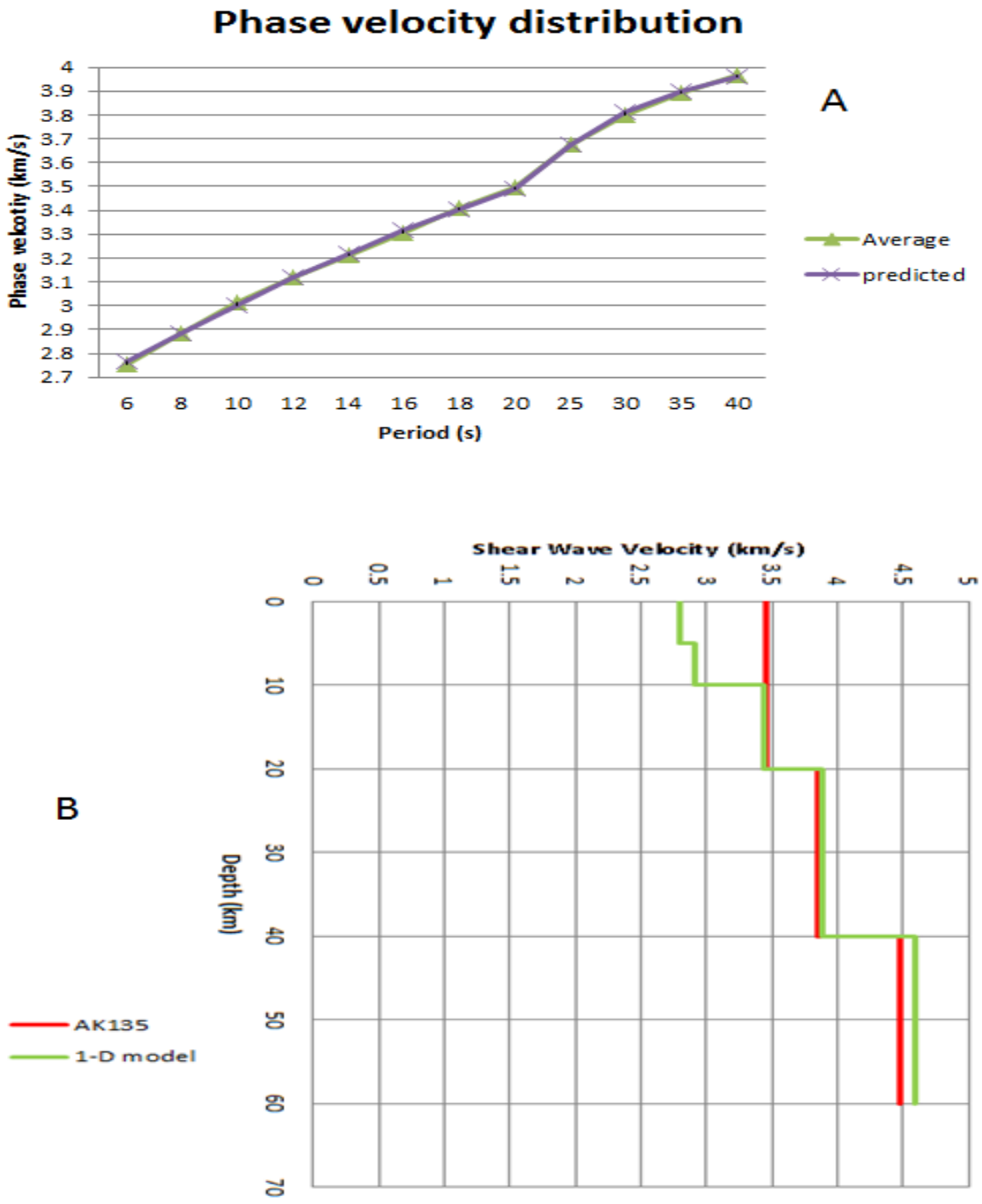

Figure 24 – 1-D Shear-wave velocity model from this study from the inversion of phase velocity by Ambient Noise Seismic Rayleigh wave tomography. (A) Average phase velocity and predicted phase velocity from the inversion shear-wave velocity. (B) Initial AK135 model and 1-D inversion shear-wave velocity model.

The 3-D shear-wave velocity model is shown in Figure 25 as velocity anomaly maps in crust and uppermost mantle. Within the crust, positive anomaly in the northwest correlating with the Laurentia craton is separated from negative anomaly in the southeast in the coast plain and the boundary is right along the Ouachita belt. The Llano Uplift area is characterized by the highest shear-wave velocity. The lowest velocity in the upper crust is imaged in the East Texas Basin and in southeastern corner of Texas, where sediment thickness is greater than 10 km (Keller and Shurbet, 1975). The lowest velocity in the southern end of Texas extends to lower crust and upper mantle. The image in the uppermost mantle shows a different velocity pattern as in the crust. The lateral variation of velocity is significantly smaller than in the crust. The boundary between the fast and slow mantle does not follow the Ouachita Belt on the surface. In addition, the most positive anomaly is much broader than the Llano Uplift and the most negative anomaly is still in the southern most of Texas.

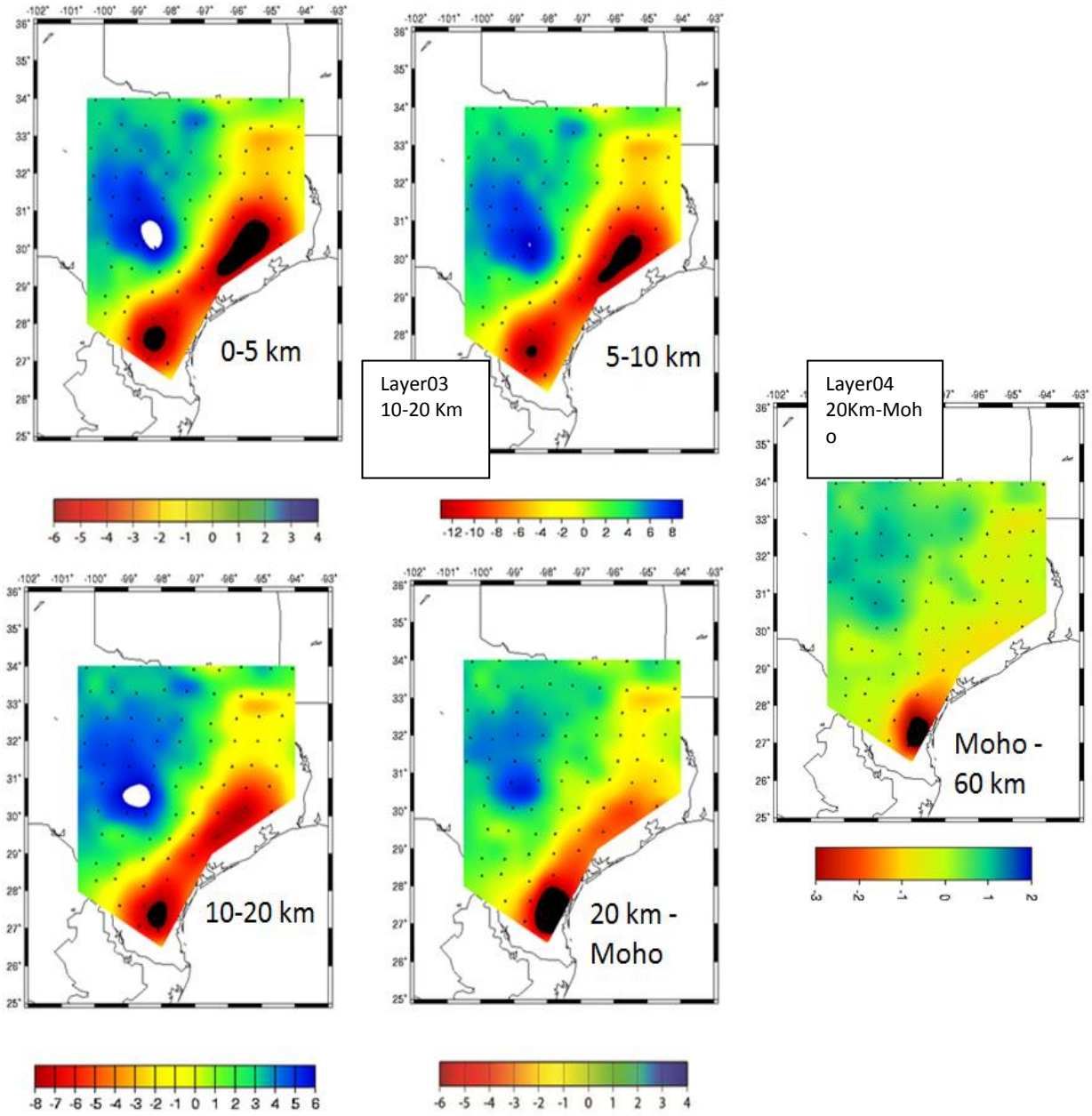

Figure 25 – 3-D Shear-wave velocity anomaly map from crust of East Texas in percentage from Ambient Noise Seismic data of TA network. Black dots are the distribution of TA stations. Layer 1 and layer 2 are upper crust contained sediment from 0 to 5 Km and 5 to 10 Km respectively. Layer 3 is middle crust from 10 to 20 Km. Layer 4 is lower crust from 20 km to Moho. Depth of layer 5 is from Moho to 60 Km.

9. Discussion

The main features of the phase velocity and shear-wave velocity maps in central and eastern Texas include the high velocity anomaly in the northwest, the low velocity anomaly in the southeast along the coast of the Gulf Mexico, and a clear boundary between these two opposite anomalies. This result made a perfect coincidence with the gravity and magnetic anomaly map (Figure 8) and geological provinces in central and eastern Texas. Compared with Figure 2, the crust of the Laurentia craton is characterized by positive anomaly while the crust of the continental margin is slow. The boundary between the positive and negative anomaly is perfectly consistent with the Ouachita Belt in the crust.

The highest velocity area corresponds to the Llano Uplift from upper to lower crust. According to the model by Mosher (2008), accompanied with subduction, collision, and another subduction, the Llano Uplift is consisted by younger granite, old granite, and serpentinite due to igneous influence. With these igneous rocks, the shear-wave velocity beneath the Llano Uplift should be definitely higher than the surrounding crust that has normal composition or thick sediment rocks.

On the phase velocity maps at periods of 10 to 30 s, beside the Llano Uplift, we also found small patches of positive anomalies along the Ouachita Belt in eastern, northeastern, and southern Texas. These anomalies well correlate with the Waco uplift, the Benton uplift, and the Devils River uplift as shown in Figure 10. Rayleigh waves at 10 to 30 s are primarily sensitive to 10 to 30 km depth, indicating these uplifts buried under sediments could have extended in mid and lower crust. However, these small-scale features are not observed on the 3-D shear-wave model, which could be due to thick layers we used in the model that smeared out the weak anomaly. In

addition, a priori constraint is used in setting the thickness of the sediment rocks in the inversion for 3D velocity, which could contribute the low resolution for the small-scale positive anomalies in the final 3D model. Further modification and improvement in the inversion method is needed for future studies.

The Ouachita Belt is a clear boundary between the positive anomaly and negative anomaly from 6 to 20 s periods. The perfect agreement between the largest velocity gradient and the Ouachita Belt disappears at longer periods, indicating the structure at depth deviates from suggested at the surface. At 30 s, a relatively slow band to the east and south of the Ouachita Belt is observed, which might be due to a relative thick crustal root associated with the Ouachita Orogeny. Since crustal thickness is not treated as a model parameter, the root beneath the Ouachita mountains, although suggested from phase velocity maps, is not resolved in the 3D model.

The slowest areas in the upper crust are located in eastern and southern Texas basin in the coastal plain, where sediment thickness is up to 12 km (Figure11) (Rosenthal and Buffler, 1987). It is also noticed that the middle part of the coastal plain is not as slow as the northern and southern part in the upper crust or on phase velocity maps from 6 to 16 s. This part is at the location of the San Marcos Arch, where basement rock is elevated than in the surrounding crust, which is reflected as relative thin sediment thickness shown in Figure 11 (Rosenthal and Buffler, 1987). The San Marcos Arch is a basement uplift formed by tectonic shortening along a northeast direction along the Gulf Coast. The southeastern trend curve in phase velocity and shear-velocity map upon San Marcos Arch coincide well with this basement thickness curve in Figure 11.

The lowest velocity in the lower crust and upper mantle in the most southern point of Texas agrees with previous study (Keller and Shurbet 1975) that imaged the upper mantle here has a slow P-wave velocity. Seismic velocity can be affected by many factors such as composition,

temperature, melt or water content, and anisotropy. As no high heat flow is detected from the southern Texas, we do not think the slow anomaly is mainly form temperature. In addition, the significance of the anomaly (greater than 6%) would require over 500℃ lateral temperature gradient in a small area in the lower crust, which is impossible. The large strength of the anomaly is also not possible from anisotropy in the crust and mantle, where weak anisotropy is generally applied. Composition change such as high volatile content could be a more plausible explanation for this anomalous slow lower crust and upper mantle. Since the area has experienced plate subduction and rifting, it is possible the subduction forming the Ouachita Orogeny could have brought old oceanic crust that contained large amount of water to the lower crust and upper mantle. Further study using long period surface waves from earthquake data is needed to image this anomaly better at depth and help to illustrate the origin of the slow anomaly.

10. Conclusion

We present here the first Texas-wide study of surface wave dispersion using ambient seismic noise method at 87 broad-band stations. By correlating year-long time series from March 2010 to February 2011 between stations, we have obtained Rayleigh wave phase velocity dispersion curves and developed phase velocity maps at periods of 6 s to 40 s. With the phase velocity data, we constructed 1-D and 3-D shear-wave velocity model with four crust layers and one upper mantle layer. The maps reveal a close correlation with major geological features. The positive anomaly area coincided with the Laurentia craton crust and the negative anomaly area coincided with the continental margin crust. The boundary between positive and negative anomaly is perfectly consistent with the Ouachita Belt. The highest velocity province is the Llano Uplift, a feature across the whole crust. The high velocity of the Llano Uplift is mainly due to the igneous influence during two Wilson Cycles. The lowest velocity in the upper crust correlates with thick sediment layers in eastern and southern Texas. And the very low velocity in southern most Texas in the lower crust and upper mantle could be due to wet oceanic crust brought to depth by subduction before the rifting in the Gulf of Mexico.

11. References

1. Bankey, V., and 17 others, 2002, Digital data grids for the magnetic anomaly map of North America, U.S. Geological Survey Open-File Report 02–414 (DVD).
2. Barmin, M. P., Ritzwoller M. H., and Levshin A. L., 2001, A fast and reliable method for surface wave tomography, Pure Appl. Geophys., v. 158(8), p. 1351–1375, doi: 10.1007/PL00001225.
3. Bassin, C., Laske, G. and Masters, G., 2000, The current limits of resolution for surface wave tomography in North America, EOS Trans AGU, v. 81, F897, 2000.
4. Bensen, G.D. et al., 2007, Processing seismic ambient noise data to obtain reliable broad-band surface wave dispersion measurements, Geophys. J. Int., v. 169, 1239-1260.
5. Bensen, G.D., Ritzwoller, M.H., Shapiro, N.M. and Levshin, A.L., 2005. Extending ambient noise surface wave tomography to continental scales: application across the United States, EOS Trans AGU, v. 86(52), Fall Meeting Suppl., Abstract S31A-0274.
6. Bird, D.E., Bruke, K., Hall, S.A., and Casey, J.F., 2005, Gulf of Mexico tectonic history: Hotspot traces crustal boundaries and early salt distribution, American Association of Petroleum Geologists Bulletin, v. 89, p. 311–328, doi: 10.1306/10280404026.
7. Bureau of Economic Geology, the University of Texas at Austin, 1997, Tectonic Map of Texas.
8. Bureau of Economic Geology, the University of Texas at Austin, 2005, Oil and Gas Map of Texas.

9. Campillo, M. and Paul, A., 2003, Long-range correlations in the diffuse seismic coda, Science, v. 299, p. 547–549.
10. Cram, I.H., Jr., 1962, Crustal structure of Texas coastal plain region, American Association of Petroleum Geologists Bulletin, v. 46, p. 1721–1727.
11. Culotta, R., et al., 1992, Deep structure of the Texas Gulf passive margin and its Ouachita-Precambrian basement: results of the COCORP San Marcos Arch Survey, The American Association of Petroleum Geologists Bulletin, v. 76(2), p. 270-283.
12. Derode, A., Larose, E., Tanter, M., de Rosny, J., Tourim, A., Campillo, M. and Fink, M., 2003, Recovering the Green's function from field-field correlations in an open scattering medium, J. Acoust. Soc. Am., v. 113, p. 2973–2976.
13. Dorman, J., Worzel, J. L. et al., Crustal section from seismic refraction measurements near Victoria, Texas, Geophysics, v. 37, p. 325-336.
14. Dziewonski, A.M., Bloch, S. and Landisman, M., 1969. A technique for the analysis of transient seismic signals, Bull. Seism. Soc. Am., v. 59, p. 427–444.
15. Evans, S. L., and Zoerb, R. M., 1984, Possible relationships between deep structure and shallow fault patterns, northwest Maverick Basin, Val Verde County, Texas, in Stratigraphy and structure of the Maverick Basin and the Devil's River uplift, Kinney and Val Verde Counties, Texas, American Association of Petroleum Geologists-Society of Economic Paleontologists and Mineralogists Annual Meeting, San Antonio Geological Society Guidebook, P. 94-98.
16. Gao, S.S., Liu, K.H., Stern, R.J., Keller, R.G., Hogan, J.P., Pulliam, J., and Anthony, E.Y., 2008, Characteristics of mantle fabric beneath the south-central United States: Constraints from shear-wave splitting measurements, Geosphere, v. 4, p. 411–417.

17. Hales, A.L., Helsley, C.E., and Nation, J.B., 1970, Crustal structure study of the Gulf Coast of Texas, American Association of Petroleum Geologists Bulletin, v. 54, p. 2040–2057.
18. Huerta, A.D., and Harry, D.L., 2012, Wilson cycles, tectonic inheritance, and rifting of the North American Gulf of Mexico continental margin: Geosphere, v. 8, p. 374-385, doi: 10.1130/GES00725.1.
19. Karim G. Sabra et al., 2005, Extracting time-domain Green's function estimates from ambient seismic noise, Geophys. Res. Lett, v. 32, L03310, doi: 10.1029/2004GL021862.
20. Keller, G.R., Braile, L.W., McMechan, G.A., Thomas, W.A., Harder, S.H., Chang, W.F., and Jardine, W.G., 1989, Paleozoic continent-ocean transition in the Ouachita mountains imaged from PASSCAL wide-angle seismic reflectionrefraction data, Geology, v. 17, p. 119–122, doi: 10.1130/0091-7613(1989)017..
21. Keller, G.R., and Cebull, S.E., 1973, Plate tectonics and the Ouachita System in Texas, Oklahoma, and Arkansas, Geological Society of America Bulletin, v. 83, p. 1659-1666.
22. Keller, G.R., and Shurbet, D.H., 1975, Crustal structure of the Texas Gulf Coastal Plain, Geological Society of America Bulletin, v. 86, p. 807–810, doi: 10.1130/0016-7606(1975)86<807: CSOTTG> 2.0.CO;2.
23. Kennett B.L.N., Engdahl E.R. and Buland R., 1995, Constraints on seismic velocities in the earth from travel times, Geophys. J. Int., v. 122, p. 108-124.
24. Lillie, R. J., Nelson, K. D. et al., 1983, Crustal structure of Ouachita Mountains, Arkansas; A model based on integration of COCORP reflection profiles and regional geophysical data, American Association of Petroleum Geologists Bulletin, v. 67, p. 907-931.

25. Lin, F., Moschetti, M. P. and Ritzwoller M. H., 2008, Surface wave tomography of the western United States from ambient seismic noise: Rayleigh and Love wave phase velocity maps, Geophys. J. Int., v. 173(1), p. 281–298, doi: 10.1111/j.1365 - 246X.2008.03720.x.
26. Lin, F. C., Ritzwoller, M.H., Townend, J., Savage, M. and Bannister, S., 2007, Ambient noise Rayleigh wave tomography of New Zealand, Geophys. J. Int., in press.
27. Mickus, R.J. Stern et al., 2009, Potential field evidence for a volcanic rifted margin along the Texas Gulf Coast, Geology, v. 37, p. 387-390, doi: 10.1130/G25465A. 1.
28. Mitchell, B. J., and Landisman, M., 1970, Interpretation of a crustal section across Oklahoma, Geological Society of America Bulletin, v. 81, p. 2647-2656.
29. Moschetti, M.P., Ritzwoller, M.H. and Shapiro, N.M., 2007, Ambient noise tomography from the first two years of the USArray Transportable Array: group speeds in the western US, Geophys. J. Int.
30. Mosher, S., et al., 2008, Mesoproterozoic plate tectonics: A collisional model for the Grenville-aged orogenic belt in the Llano uplift, central Texas, Geology, v. 36, p. 55-58, doi: 10.1130/G24049A.1.
31. Nelson, K. D., Lillie, R. J. et al., 1982, COCORP seismic reflection profiling in the Ouachita Mountains of western Arkansas; Geometry and geologic interpretation, Tectonics, v. 1, p. 413-430.
32. Nicholas, R.L., and Rozendal, R.A., 1975, Subsurface positive elements within the Ouachita foldbelt in Texas and their relation to Paleozoic craton margin, American Association of Petroleum Geologists Bulletin, v. 459, p. 193–216.

33. Prewitt, R. H., 1969, Crustal thickness in central Texas as determined by Rayleigh wave dispersion (M.S. thesis), Lubbock, Texas Tech University, 69 p.
34. Raye, U et al., 2011, Composition of the mantle lithosphere beneath south-central Laurentia: Evidence from peridotite xenoliths, Knippa, Texas Geosphere, EISSN 1553-040X, v. 7(3), p. 710–723.
35. Rosenthal, D.B., and Buffler, R.T., 1987, Depth to basement Gulf of Mexico region, University of Texas Institute of Geophysics Map, scale 1:2,500,000.
36. Sabra, K.G., Gerstoft, P., Roux, P., Kuperman, W.A. and Fehler, M.C., 2005b. Surfacewave tomography from microseism in southern California, Geophys. Res. Lett., v. 32, p. 143-154, doi: 10.1029/2005GL023155.
37. Saito, M., (1988), DISPER80: a subroutine package for the calculation of seismic normal-mode solutions, in D.J. Doornbos ed., Seismological Algorithms, p. 293– 319.
38. Salvador, A., 1991a, Origin and development of the Gulf of Mexico basin, in Salvador, A., ed., The Gulf of Mexico Basin: Boulder, Colorado, Geological Society of America, Geology of North America, v. J, p. 389–444.
39. Salvador, A., 1991b, Triassic-Jurassic, in Salvador, A., ed., The Gulf of Mexico Basin: Boulder, Colorado, Geological Society of America, Geology of North America, v. J, p. 131–180.
40. Shapiro, N.M. and Campillo, M., 2004. Emergence of broadband Rayleigh waves from correlations of the ambient seismic noise, Geophys. Res. Lett, v. 31, p. 76-90, doi: 10.1029/2004GL019491.
41. Shapiro, N.M., Campillo, M., Stehly, L. and Ritzwoller, M.H., 2005, High resolution surface wave tomography from ambient seismic noise, Science, v. 307, p. 1615–1618.

42. Shapiro, N.M. and Ritzwoller, M.H., 2002, Monte-Carlo inversion for a global shear velocity model of the crust and upper mantle, Geophys. J. Int., v. 151, p. 88–105.
43. Stewart, S.W., 1968, Crustal structure in Missouri by seismic-refraction methods, Seismological Sociedty of America Bulletin, v. 58, p. 291-323.
44. Thomas, W., 1976, Evolution of the Ouachita-Appalachian continental margin, Geology, v. 84, p. 323–342.
45. Thomas, W.A., 1991, The Appalachian-Ouachita rifted margin of southeastern North America, Geological Society of America Bulletin, v. 103, p. 415–431, doi: 10.1130/0016-7606(1991)103<0415:TAORMO>2.3.CO;2.
46. Warren, D. H., 1968, Transcontinental geophysical survey (35 – 39 N) seismic refraction profiles of the crust and upper mantle from 74 to 87 W longitude, U.S. Geological Survey Miscellaneous Geological Investigations Map I-535-D, scale 1:1,000,000.
47. Weaver, R.L. and Lobkis, O.I., 2001a, Ultrasonics without a source: Thermal fluctuation correlation at MHz frequencies, Phys. Rev. Lett., v. 87, p. 211-221, doi: 10.1103/PhysRevLett.87.134301.
48. Weaver, R.L. and Lobkis, O.I., 2001b, On the emergence of the Green's function in the correlations of a diffuse field, J. Acoust. Soc. Am., v. 110, p. 3011–3017.
49. Yang, Y., Ritzwoller, M.H., Levshin, A.L. and Shapiro, N.M., 2007, Ambient noise Rayleigh wave tomography across Europe, Geophys. J. Int., v. 168, p. 259–274.
50. Yao, H., van der Hilst, R.D. and de Hoop, M.V., 2006, Surface-wave tomography in SE Tibet from ambient seismic noise and two-station analysis: I.—Phase velocity maps, Geophys. J. Int., v. 166, p. 732–744, doi: 10.1111/j.1365–246X.2006.03028.x.